Active vibration control of mechanical servo high speed fine-blanking press

Yan xiong Liu
"Wuhan University of Technology"
Yuwen Shu (1543380083@qq.com)
"Wuhan University of Technology" https://orcid.org/0000-0001-5703-6766
Wen tao Hu
"Wuhan University of Technology"
Xin hao Zhao
"Wuhan University of Technology"
Zhi cheng Xu
"Wuhan University of Technology"

Original Article

Keywords: Mechanical servo high speed fine-blanking press, Active vibration control, Self-adaptive feed forward control, Matlab

Posted Date: April 2nd, 2020

DOI: https://doi.org/10.21203/rs.3.rs-19728/v1

Version of Record: A version of this preprint was published at Strojniški vestnik – Journal of Mechanical Engineering on September 15th, 2021. See the published version at https://doi.org/10.5545/sv-jme.2020.6959.

Title page

Active vibration control of mechanical servo high speed fine-blanking press

Yan-Xiong Liu, born in1985, Associate Professor, School of automotive engineering, *Wuhan University of Technology*, *Hubei Key Laboratory of Advanced Technology of Automotive Components.*; E-mail: liuyx@whut.edu.cn.

Yu-Wen Shu, born in 1997, Graduate student, School of automotive engineering, *Wuhan University of Technology, Hubei Key Laboratory of Advanced Technology of Automotive Components.*;E-mail:1543380083@qq.com

Wen-Tao Hu, born in 1995, Graduate student, School of automotive engineering, *Wuhan University of Technology, Hubei Key Laboratory of Advanced Technology of Automotive Components.*; E-mail: wentaohu.whut@qq.com

Xin-Hao Zhao, born in 1989, Ph.D. School of automotive engineering, *Wuhan University of Technology, Hubei Key Laboratory of Advanced Technology of Automotive Components.*; E-mail: zhaoxh@whut.edu.cn

Zhi-Cheng Xu, born in 1994, Ph.D. School of automotive engineering, *Wuhan University of Technology, Hubei Key Laboratory of Advanced Technology of Automotive Components.*; E-mail: Xuzhicheng@whut.edu.cn

Corresponding author: Yu-Wen Shu E-mail: 1543380083@qq.com

ORIGINAL ARTICLE

Active vibration control of mechanical servo high speed fine-blanking press

Yanxiong Liu[1,3], Yuwen Shu, Wentao Hu, Xinhao Zhao*[1,2], Zhicheng Xu[1,3]

1.Hubei Key Laboratory of Advanced Technology of Automotive Components, Wuhan University of Technology, Wuhan, 430070, China.

2. School of Materials Science and Engineering, Wuhan University of Technology, Wuhan, 430070, China.

3.Hubei Collaborative Innovation Center for Automotive Components Technology, Wuhan University of Technology, Wuhan 430070, China.

Abstract: The fine-blanking process as an advanced sheet metal forming process has been widely applied in the industrial area. However, special designed equipment is required for this process. In this paper, a novel mechanical servo high speed fine-blanking press with the capacity of 3200kN is proposed, and the vibration control for this machine is researched to achieve the requirement of fine-blanked parts of high dimensional accuracy, since the vibration of the fine-blanking machine will cause the machining displacement error and reduce the machining accuracy. The self-adaptive feed forward control is used to simulate the active vibration control of the mechanical fine-blanking machine. The vibration control principle of the fine-blanking machine is described and the control algorithm is established. At the same time, the vibration mechanical model of the fine-blanking machine as the controlled object is established, and the parameters of the excitation input and the mechanical model are obtained by the fine-blanking finite element simulation and the experiments of the vibration measurement of the press. Finally, the numerical simulation and analysis of active vibration control based on Matlab are carried out. The results show that the control effect is good, and the vibration response is effectively reduced.

Keywords: **Mechanical servo high speed fine-blanking press; Active vibration control; Self-adaptive feed forward control; Matlab**

1. Introduction

The fine-blanking (FB) process as an advanced net shape or near net shape plastic forming process has been widely applied in the industrial area since of the

* Corresponding author. E-mail address: 1543380083@qq.com

advantages of high efficiency and high parts quality [1], [2]. Lots of mid-thick sheet metal components with complicate shape and high dimensional accuracy can be fabricated by the FB process in one operation as shown in Fig.1a. Compared with the conventional blanking process, a special designed fine-blanking press was required for this process, which can provide at least three separately forces, namely blanking force, blank holder force and counter punch force [3]. Now, almost all of the FB press is hydraulic machine with the capacity of 3200kN ~ 12000kN [4], and the forming efficiency is about 30~70 times per minute with punch stroke of 40mm. With the increasing of huge market demand for the mid-thick sheet metal parts, the FB efficiency should be further improved, which the target is about 200 times per minute or higher.

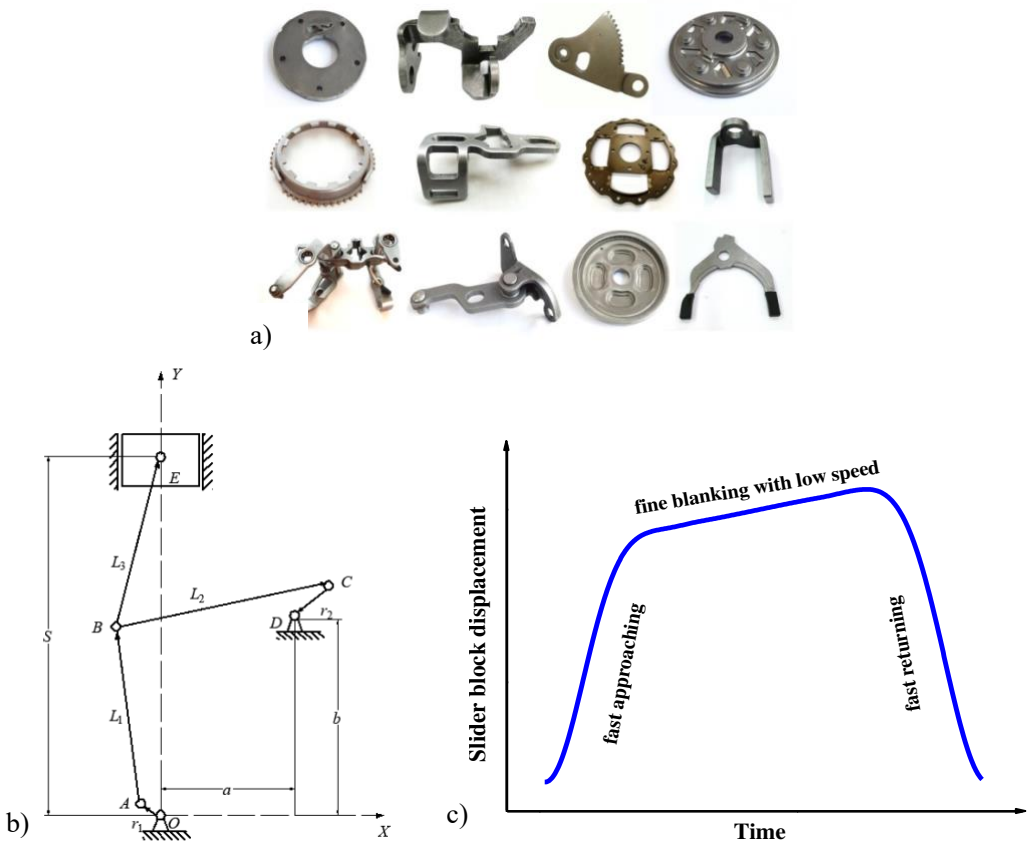

Fig.1. a) the mid-thick sheet metal parts fabricated by FB process, b) the mechanical construction of the main driving system of the high speed FBFB press and c) the slide block stroke diagram.

A mechanical servo high speed FB press was designed and fabricated by our research group and Huangshi Huali Co., Ltd., and the forming efficiency can reach up to 220 times per minute and the maximum forming capacity is 3200kN. The mechanical construction of the main driving system is shown in Fig.1b, and the main

slide block can get the trajectory as shown in Fig.1c.. With the increasing of the punch frequency, the vibration of the FB press will become more and more severe. It is known that the vibration of the press not only affects the parts quality, such as causing the crack on the cutting surface and reduce the dimensional accuracy, but also reduce the service life of the machine. Moreover, the noise caused by the machine vibration will deteriorate the working condition and affect the human health. However, the research on the vibration control of mechanical FB press is blank. Therefore, the vibration control for the high speed fine blanking press is urgently required.

In general, the passive control method was applied for the vibration control of the traditional press, such as increasing the stiffness of the frame and adding the vibration isolation system, and the vibration control effort for the excitation source of the press is very rare. For the high speed FB press proposed in this paper, except of the passive control method, the active vibration control method was also applied to restrain the vibration of the whole machine caused by the elastic restoring force produced by the FB process. Therefore, the low-frequency vibration can be effectively suppressed, and so as to reduce the vibration of the mechanical servo high speed FB press at the greatest extent.

For the research of the active control, Paul published the first patent for the active noise control in 1936. The basic idea is that using the active control wave with the same amplitude of the noise to counteract the original noise. In 1953, Olson invented the electronic sound absorption equipment, which proved that the practical feasibility of the active vibration and noise control theory through experiments. Then, the active vibration control technology has been gradually applied into the engineering machine. Mitsuhashi et al. applied the active vibration system to the diesel engine. Winberg et al. (2012) and Daley et al. applied the active vibration control for the marine applications [5], [6].

In recent years, a lot of new active vibration control theories were developed. Shao and Zhang created the finite element (FE) active vibration control model the piezoelectric flexible linkage by using the mixed Hamilton principle [7]. Based on the complex mode theory, a hybrid independent mode controller which consisted of the state feedback and disturbance feed forward control was developed. The results show that the vibration was effectively suppressed for the flexible four-bar linkage. Li and Hu studied the active control of submarine vibration system, and the corresponding adaptive control method was put forward. A good control effect of the vibration

system by applying the periodic excitation force was obtained [8]. Zhu proposed the active vibration control process for the marine diesel engine, and the x-LMS algorithm based on the off-line identification of error channel was used to for the active vibration control [9]. Valiantsin studied and brought forward A combined bilateral and binaural active noise control algorithm for closed-back headphones. Tukesh published Active vibration control of ship mounted flexible rotor-shaft-bearing system during seakeeping. Yik R. Teo published Optimal integral force feedback for active vibration control in 2015 [10]. Park Young-min studied Semi-active vibration control of space truss structures by friction damper for maximization of modal damping ratio in 2013 [11].

Through the inspiration of the active vibration control method mentioned above, active vibration control strategy was researched for the mechanical servo high speed FB press to suppress the periodic low-frequency vibration of the machine. The active vibration control principle of high speed FB press was analyzed, and the adaptive vibration controller was created. According to test results of the FB press vibration, the input parameters for the control model were obtained, and the active vibration control effect was predicted by using the Matlab.

2 Adaptive vibration controller design

2.1 Active vibration control system

The active vibration control system of mechanical servo FB press is mainly composed of the following parts as shown in Fig.2 .

(1) Controlled object. In this paper, the controlled object is the mechanical servo FB press. The main drive system of the press is the excitation source of controlled object, the excitation force acts on the frame, and then transfers to the whole machine. Since the elastic restoring force is mainly acted in the vertical direction, the mathematical model of the controlled object is mainly focused on the vertical deformation.

(2) Measuring mechanics. The core component of the measuring mechanics is the sensor. Acceleration sensor is often used in the data acquisition of vibration response. The vibration signal of the whole machine measured by the acceleration sensor is transmitted to the control system through signal amplification and filtering, which used as the input parameter of the active vibration control.

(3) Electric actuator. According to the command of the controller, the actuator

applies the specified force or torque on the frame of the press, and feeds back the action effect to the controller.

(4) Controller. The controller is the core part of the active vibration control system, which can provide the command and control rate of the actuator. Because the main driving system is motorial during the forming process, the adaptive controller which can adjust the parameters of the control system is applied in this paper.

(5) Energy and auxiliaries. The external energy supplies the input energy of the actuator for the active vibration control system of the FB press.

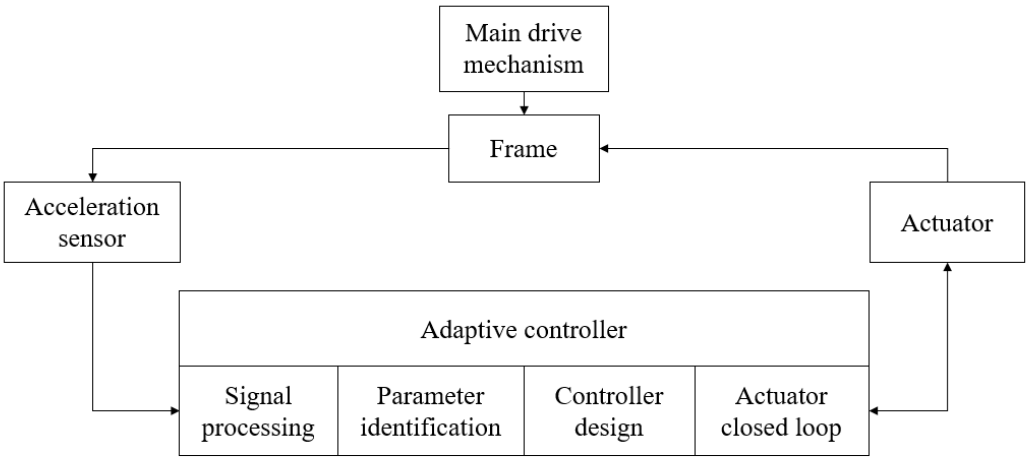

Fig.2. Schematic diagram of the active vibration control system for FB press.

2.2 Adaptive vibration control algorithm

The selection and design of the algorithm play an important role in the adaptive vibration controller. Among many adaptive control methods, the Least Mean Square (LMS) adaptive algorithm has been widely used [12], which using the gradient search method, the convergence solution can be obtained quickly, and the implementation is relatively simple.

The LMS algorithm can be expressed by Eq.1.

$$F(e(n)) = \varepsilon(n) = E(e^2(n)) = E\left[d^2(n) - 2d(n)y(n) + y^2(n)\right] \tag{1}$$

The filter of the adaptive active vibration controller adopts the FIR structure, and its structure diagram is shown in Fig.3.

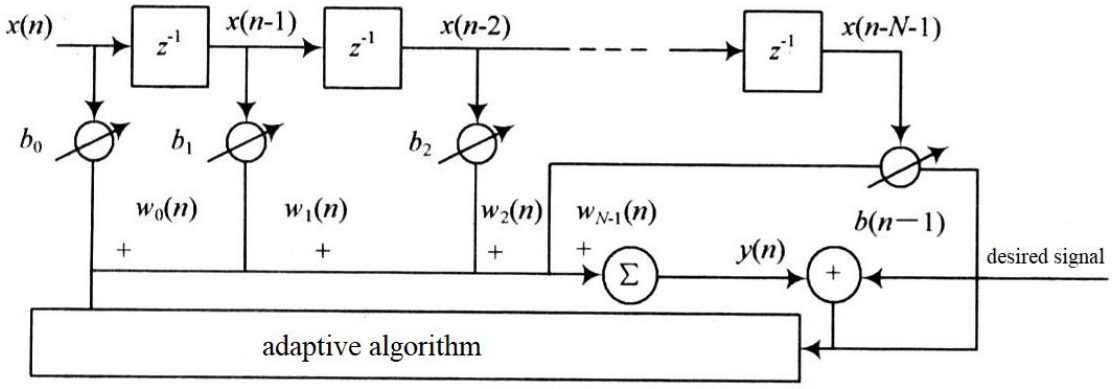

Fig.3. Adaptive FIR filter.

where x(n) is the input of the adaptive active vibration control filter, y(n) is the output of the adaptive active vibration control filter, w (n) is the impulse response, w (n) = {w (0), w (1,... , w (n-1)}, then:

$$y(n) = \mathbf{W}^T(n)\mathbf{X}(n) = \sum_{i=0}^{N-1} w_i(n)x(n-i) \tag{2}$$

For the filter with transverse structure, substitute the expression of y(n) into Eq.1:

$$\varepsilon = E(\mathbf{d}^2(n)) + \mathbf{W}^T(n)\mathbf{R}\mathbf{W}(n) - 2\mathbf{W}^T(n)\mathbf{P} \tag{3}$$

where $\mathbf{R} = E\left[\mathbf{X}(n)\mathbf{X}^T(n)\right]$ is the autocorrelation matrix of N×N, $\mathbf{P} = E\left[\mathbf{d}(n)\mathbf{X}(n)\right]$ is the cross-correlation vector for N×1 which represents the correlation between the ideal signal d(n) and the input vector.

Because the gradient descent method is adopted for the optimization process, so:

$$\frac{\partial \varepsilon}{\partial \mathbf{W}(n)_{w(n)=w^*}} = 0 \tag{4}$$

When the mean square error ε reaches to the minimum value, the optimal weight coefficient can be obtained.

If the R matrix is full rank, the best value of weight coefficient should be satisfied with $\mathbf{W}^* = \mathbf{R}^{-1}\mathbf{P}$, namely:

$$\begin{bmatrix} w_0^* \\ w_1^* \\ \vdots \\ w_{(n-1)}^* \end{bmatrix} = \begin{bmatrix} \phi_x(0) & \phi_x(1) & \cdots & \phi_x(n-1) \\ \phi_x(1) & \phi_x(0) & \cdots & \phi_x(n-2) \\ \vdots & \vdots & \ddots & \vdots \\ \phi_x(n-1) & \phi_x(n-2) & \cdots & \phi_x(0) \end{bmatrix}^{-1} \begin{bmatrix} \phi_{xd}(0) \\ \phi_{xd}(1) \\ \vdots \\ \phi_{xd}(n-1) \end{bmatrix} \tag{5}$$

Where, $\phi_x(m) = E\left[x(n)x(n-m)\right]$ shows the autocorrelation value of $x(n)$, $\phi_{xd}(k) = E\left[x(n)d(n-k)\right]$ represents the cross-correlation value between $x(n)$ and $d(n)$.

In practical applications, it is difficult to obtain the autocorrelation and cross-correlation values of signals. Therefore, gradient estimation value can be used, that is:

$$\hat{g}_w(n) = -2d(n)x(n) + 2x(n)x^T(n)w(n) = 2x(n)(-d(n) + x^T(n)w(n)) \tag{6}$$

Using the gradient estimation value to replace the real values. then:

$$w(n+1) = w(n) + 2\mu e(n)x(n) \tag{7}$$

This is the iterative equation of LMS algorithm. In practical application, the step size is fixed, and the value of μ will affect the performance of the algorithm, resulting in the change of convergence speed, jump tracking ability and steady-state imbalance of the algorithm. Since the most appropriate μ value is very hard to be obtained, the variable step size normalized LMS algorithm is usually applied, which can be expressed as:

$$w(n+1) = w(n) + 2\mu_n e(n)x(n) = w(n) + \Delta w(n) \tag{8}$$

According to the expression of instantaneous square error of LMS algorithm, the instantaneous square error of variable step size normalized LMS algorithm can be expressed as:

$$\begin{aligned} \tilde{e}^2(n) &= e^2(n) + 2\Delta w^T(n)x(n)x^T(n)w(n) \\ &+\Delta w^T(n)x(n)x^T(n)w(n) - 2d(n)\Delta w^T(n)x(n) \end{aligned} \tag{9}$$

Then:

$$\Delta e^2(n) = \tilde{e}^2(n) - e^2(n) = -2\Delta w^T(n)x(n)e(n) + \Delta w^T(n)x(n)x^T(n)w(n) \tag{10}$$

From $\Delta w(n) = 2\mu_n e(n)x(n)$, we can get:

$$\Delta e^2(n) = -4\mu_n e^2(n)x^T(n)x(n) + 4\mu_n e^2(n)\left[x^T(n)x(n)\right]^2 \tag{11}$$

To minimize $\Delta e^2(n)$, which make the instantaneous square error close to the square error, we can take $\frac{d\Delta e^2(n)}{d\mu_n} = 0$, then

$$\mu_n = \frac{1}{2x^T(n)x(n)} \tag{12}$$

In order to avoid the steady-state misadjustment, a fixed numerical convergence factor μ_k is introduced to avoid large step size when the denominator is very small during the iteration process. At the same time, another parameter γ is introduced to adjust the denominator. Then the updated iterative equation of the new variable step size normalized LMS algorithm is:

$$w(n+1) = w(n) + \frac{\mu_k}{\gamma + x^T(n)x(n)} e(n)x(n) \tag{5-13}$$

2.3 Adaptive feedforward active vibration control of the fine blanking press

As mentioned in section 2.1, the main drive system of the press applies vertical excitation force to the whole machine, including the frame. The actuator is installed on the frame, which can exert a controllable force with the opposite direction of the excitation force of main drive system to offset the original vibration and realize active vibration reduction.

Because the vibration on the frame is easy to measure, the upper and lower crossbeams of the frame are selected as the vibration observation parts of the control system. The excitation force *F*(n) generated by the main drive system is transmitted to the frame through the primary channel to generate the vibration response d(n), which can be used as the reference input of the adaptive active vibration control. *R*(n) is the control input, and the value is the estimated value of the excitation force. By adjusting the *R*(n) with adaptive feedforward control method, the vibration response of the frame can be reduced, and the effect of reducing the vibration of the whole machine can be achieved. The control block diagram is shown in Fig.4.

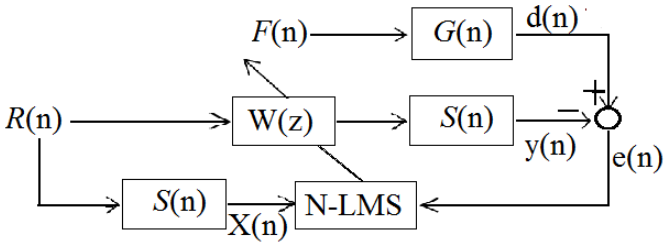

Fig.4. Active vibration control block diagram of the FB press.

In the Fig.4, *F*(n) is the excitation force generated by the main drive system, d(n) is the excitation force response used as the reference input, e(n) is the control system error and also used as the controlled output when the control system is stable, *W*(z) is the adaptive controller, *R*(n) is the estimated value of the excitation force, *G*(n) is the transfer function which reflects the excitation force transferred to the frame, *S*(n) is the transfer function which reflects the control force transferred to the frame. The FIR filter described above is adopted as the filter.

Based on the above control block diagram, the mean square error of the whole control system can be expressed as:

$$F(e(n)) = \varepsilon(n) = E(e^2(n)) = E\left[d^2(n) - 2d(n)y(n) + y^2(n)\right] \tag{14}$$

Then the control output $y(n)$ of the nth order filter is equal to the convolution operation:

$$y(n) = S(n) * \sum_{i}^{N} w(n)R(n) = \int_{0}^{\infty} S(n-\tau) * (\sum_{i}^{N} w(\tau)R(\tau)) \tag{15}$$

Then the gradient value of the mean square error can be calculated as:

$$g_w = \frac{dE\left[e^2(n)\right]}{dw} = -E\left[2e(n)S(n)R(n)\right] \tag{16}$$

According to the variable step size normalized LMS algorithm, the variable step size factor μ needs to be transformed, that is:

$$\mu = \frac{1}{2(S(n)R(n))^T (S(n)R(n))} \tag{17}$$

Then the iterative equation of the weight updating of the adaptive control algorithm can be obtained:

$$w(n+1) = w(n) + \frac{\mu_n}{\gamma + x^T(n)x(n)} e(n)x(n) \tag{18}$$

Where, $X(n) = S(n)R(n)$.

2.4 Vibration mechanical model of the fine blanking press

For the adaptive active vibration control system of fine blanking machine, it is required to establish the vibration mechanical model of the controlled object and obtain the transfer function of the control system. It is assumed that the material distribution before each blanking process can be restored, and the material penetration is regardless. The punching force is located in the vertical direction, so the vertical direction which has the maximum deformation is mainly considered. Therefore, the structure of the FB press can be expressed as a combination of linear spring dampers.

Then the vibration mechanical model as shown in Fig.5 can be established, and the motion equation for each mass block can be expressed as follows.

$$m_i \ddot{x}_i = \sum F_i^{imp} + \sum F_i^{el} \tag{19}$$

where F_i^{imp} is the sum of the impact forces exerted on the mass m_i, F_i^{el} is the sum of the elastic forces applied to the mass m_i.

The excitation source of the whole press comes from the main drive system. The excitation force acting on the main drive system is mainly composed by two parts. One part is the unbalanced inertia force F_y generated by the main drive system itself. The other part mainly is the elastic restoring force from the main drive system at the

ending of FB process, which is relatively difficult to be got, and can be obtained with the FE simulation of the FB process. The FB FE model is shown in Fig.5. The material for this simulation is TC4 titanium alloy with the thickness of 5mm. The diameter of the fine-blanked part is 20mm, and the FB speed is 5mm/s. The relationship between the FB force and the time can be obtained as shown in Fig.6. When the punch force acts on the workpiece, the reaction force exerts on the main drive system in the opposite direction, which reflects the changing of the impact load acting on the main drive system.

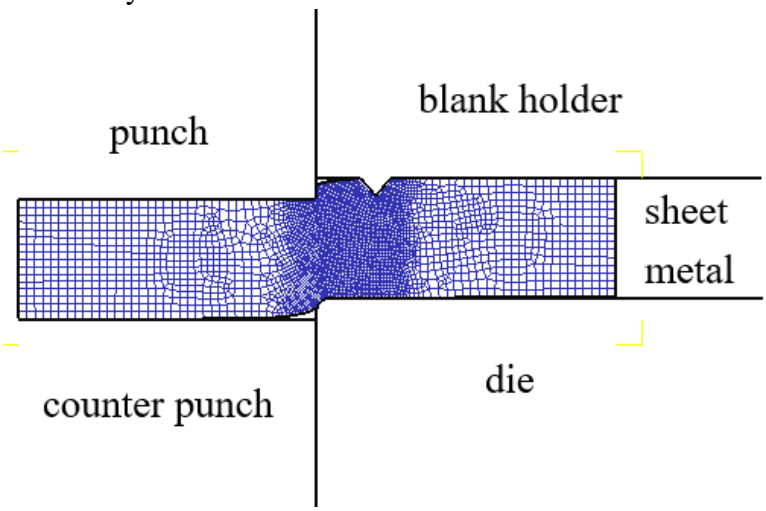

Fig.5. The FE model of the FB process.

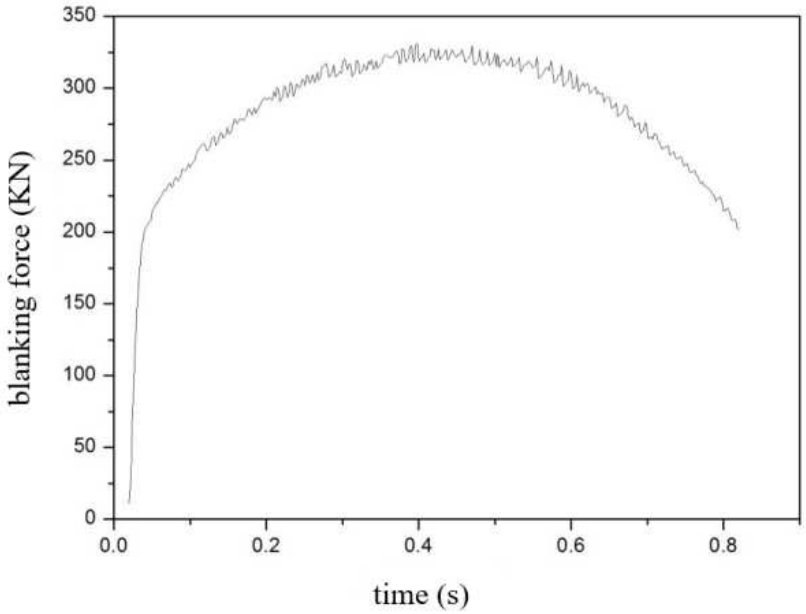

Fig.6. The relationship between the fine-blanking force and the time.

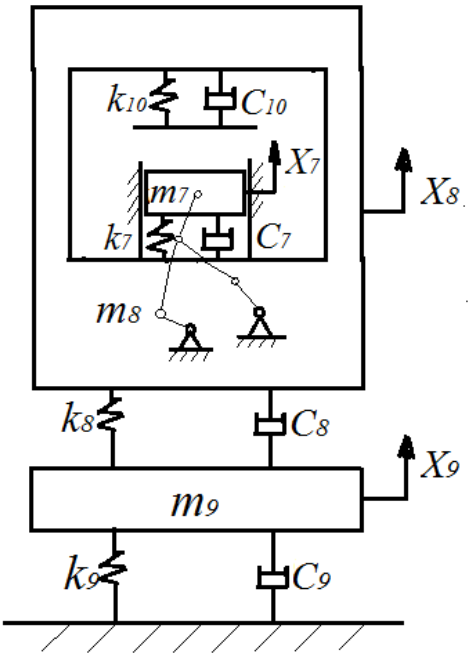

Fig.7. Vibration mechanical model of the FB press.

According to the vibration mechanical model as shown in Fig.7, the vibration equations of each mass block can be expressed by:

$$\begin{cases} m_7\ddot{x}_7 + c_7(\dot{x}_7 - \dot{x}_8) + k_7(x_7 - x_8) = F^{imp} + F_y \\ m_8\ddot{x}_8 + c_8(\dot{x}_8 - \dot{x}_9) + c_7(\dot{x}_8 - \dot{x}_7) + k_8(x_8 - x_9) + k_7(x_8 - x_7) = 0 \\ m_9\ddot{x}_9 + c_9\dot{x}_9 + c_8(\dot{x}_9 - \dot{x}_8) + k_9x_9 + k_8(x_9 - x_8) = 0 \end{cases} \tag{20}$$

where m_7, k_7, c_7 and x_7 represent the mass, equivalent stiffness, equivalent damping and displacement of the main drive, respectively. m_8, k_8, c_8 and x_8 represent the mass, equivalent stiffness, equivalent damping and displacement of the frame, respectively. m_9, k_9, c_9 and x_9 represent the mass, equivalent stiffness, equivalent damping and displacement of the embedded footings, respectively. k_{10} and c_{10} represent the equivalent stiffness and damping of the upper worktable. $\ddot{x}_j$ and $\dot{x}_j$ （j=6,7,8）represent the acceleration and velocity of the mass block.

2.4.1 Parameters determination of the vibration mechanical equation

In order to solve the vibration mechanical equation, the parameters, such as the equivalent mass, equivalent stiffness, equivalent damping value and so on, should be determined firstly based on the FB press structural.

(1) embedded footings system

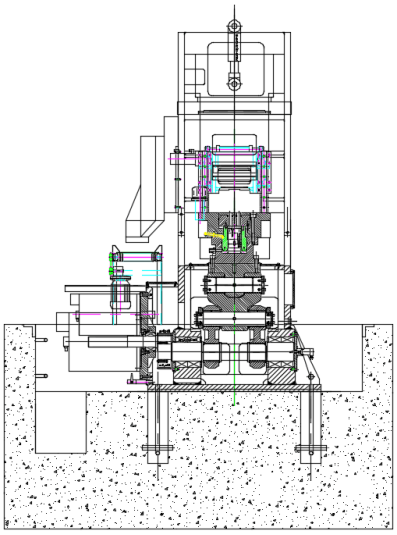

Fig.8. Foundation installation design of mechanical fine blanking machine

Fig.8 shows the foundation installation system for the FB press. For the embedded foundation in the deep homogeneous layer, we can use the formulas presented in the Ref [13] and [14] to calculate the stiffness and damping value. That is:

$$\begin{cases} k = Gr_0(C_{v1} + \dfrac{G_S}{G}\dfrac{l}{r_0}S_{v1}) \\ c = r_0^2\sqrt{\rho G}(\bar{C}_{v2} + \bar{S}_{v2}\dfrac{l}{r_0}\sqrt{\dfrac{\rho_S}{\rho}\dfrac{G_S}{G}}) \end{cases} \tag{21}$$

where G is the shear modulus of the soil, r_0 is the radius of circular foundation or the equivalent radius of non-circular foundation. ρ is the density of the soil, l is the depth of embedment, G_S and ρ_S is the shear modulus and density of the backfill side layer. Dimensionless stiffness and damping parameters C_{v1} and $\bar{C}_{v2}$ depend on the dimensionless frequency. S_{v1} and $\bar{S}_{v2}$ is the dimensionless stiffness and damping parameter of the Side layer. Novak provided the C_{v1}, $\bar{C}_{v2}$, S_{v1} and $\bar{S}_{v2}$ for most stamping equipment as shown in table 1 [15].

Table 1. Reference values of stiffness and damping for foundation installation system.

soil	Half-space		Side layer	
	C_{v1}	$\bar{C}_{v2}$	S_{v1}	$\bar{S}_{v2}$
Cohesive soil	7.5	6.8	2.7	6.7
Granular soil	5.2	5.0		

Based on the installation conditions of mechanical servo FB press, the average shear wave velocity of soil is 150m/s, and the density is 1900kg/m3. The total mass of

the foundation system is taken as 400000 kg. The average shear wave velocity of backfill material is 120m/s, and the mass density is 2400kg/m3. The shear modulus of soil can be evaluated by $G = \rho V_S^2$, and it is 42.75MPa for footing and 25.9MPa for side layer. Therefore, the stiffness and damping constants of the foundation installation system can be calculated by Eq.21, which is k = 8.1e8N/m and c = 1.1e7N/m/s.

(2) Frame part

Because of the complexity of the frame structure, the FE method is usually used to obtain the equivalent stiffness of the frame mass. As shown in Fig.9, the bottom surface is fixed by four points, and the upper crossbeam is applied with 200N uniform force to get the deformation of the frame. According to the simulation results, the maximum deformation of the frame is 6.7324e-8m. Therefore, the equivalent stiffness of the frame can be calculated by:

$$k_f = \frac{F_f}{\Delta l} = 200/6.7324\text{e-}8 = 2.971\text{e}9\text{N/m} \tag{22}$$

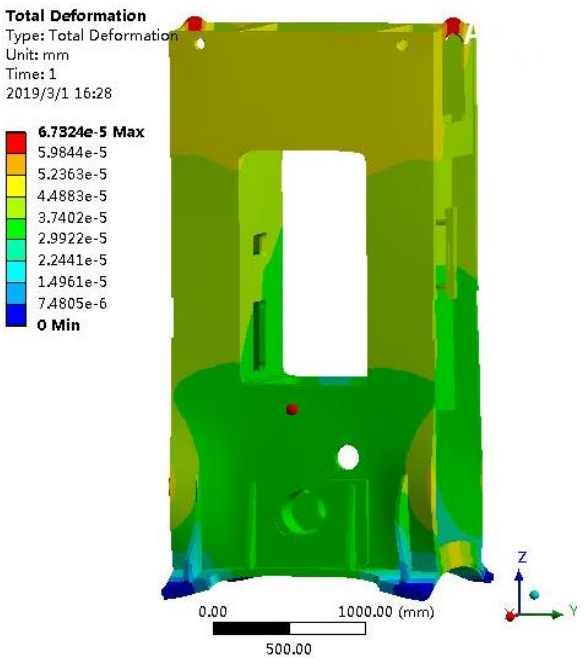

Fig.9. Frame deformation under the action of the constant load.

It is a little difficult to calculate the equivalent damping value of the frame. In general, it is required to calculate the logarithmic decrement rate δ of the system response under the impact vibration. The relationship between the logarithmic decrement rate and the structural damping ratio is shown in Eq.(23).

$$\delta = In\frac{x_i}{x_{i+T}} = \frac{2\pi\xi}{\sqrt{1-\xi^2}} \tag{23}$$

where ξ is the damping ratio of the frame, x_i is the displacement, velocity or acceleration amplitude on the frame at the time of t_i, x_{i+T} is the displacement, velocity or acceleration amplitude on the same location at the time of t_{i+T}.

Because the value of ξ is very small and can be ignored after the square. Then, Eq.(23) can be simplified as:

$$\delta = In\frac{x_i}{x_{i+T}} = 2n\pi\xi \tag{24}$$

Based on Eq.(24), once the logarithmic decrement rate δ is determined, the damping ratio ζ of the frame can be obtained.

$$c = 2\xi\sqrt{mk} \tag{25}$$

Therefore, to obtain the equivalent damping of the frame, the logarithmic decrement rate of the vibration amplitude of the system under the impact load should be calculated firstly. Based on the above FE model, 1MN impact force is applied to the frame workbench and the bearing seat hole with the lasting time of 0.02s. According to the simulation result, the maximum acceleration and velocity changing point on the frame can be obtained as shown in Fig.10.

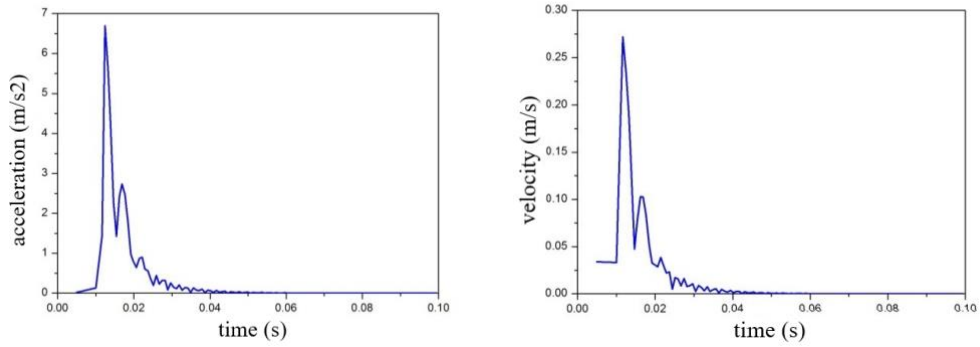

(a) acceleration (b) velocity

Fig.10. Acceleration and velocity attenuation on the frame under the impact load.

From Fig.10, the following equivalent damping parameters can be obtained and summarized in Table 2.

Table 2. Equivalent damping parameters of the frame.

	Value		Logarithmic decrement rate δ	Damping ratio of frame ξ
	t_i	t_{i+T}		
velocity v_7	0.272	0.103	0.971	0.154
acceleration	6.691	2.731	0.896	0.143

a_7

From Table 2, it can be seen that the damping ratio of the frame is near 0.15. Therefore, it can be taken as 0.15. It is also known that the total mass of the frame is 12314kg. According to the Eq.(23)-(25), the equivalent damping value of the frame can be obtained as c_7=1.81e6.

(3) Main drive system

For the main drive system, the equivalent stiffness and damping can be obtained with the same method applied for the frame part. The FE model for the main drive system was created as shown in Fig.11, in which the support constraint is applied the bearing pedestal at the bottom of the main drive system, and the horizontal displacement of the slide block is constrained. The deformation of the main drive system can be obtained by applying 200N uniform force load on the top of the slider as shown in Fig.11.

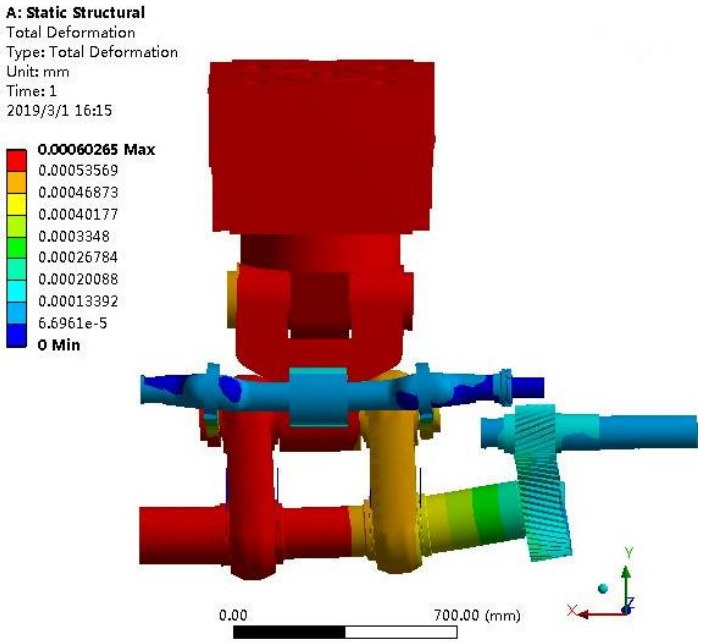

Fig.11. Deformation of the main drive system under the constant load.

It can be seen from Fig.10 that the maximum deformation of the main drive system under the constant load is 6.0265e-7m. Then, the equivalent rigidity of the main drive system can be obtained by Eq.(26)

$$k_T = \frac{F_T}{\Delta l} = 200/6.0265\text{e-}7 = 3.32\text{e}8\text{N/m} \tag{26}$$

In order to get the equivalent damping of the main drive system, the 10e5n impact for is applied to the top surface of the slider for 0.02s. The maximum acceleration and velocity changing point on the main drive system can be obtained from the simulation results as shown in Fig.12.

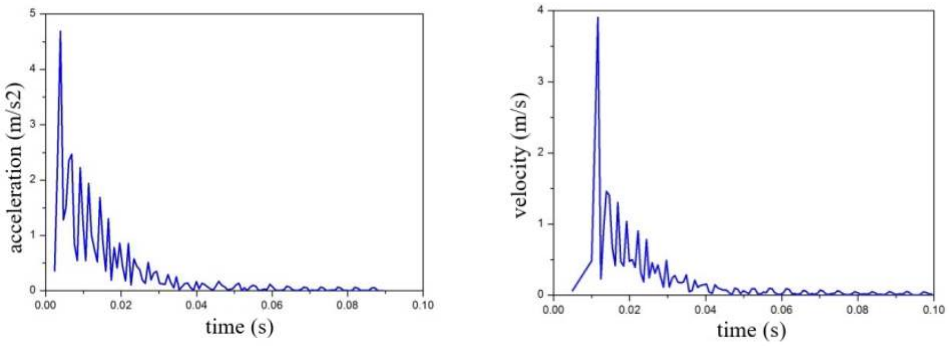

(a) acceleration (b) velocity

Fig.12. Acceleration and velocity attenuation of the main drive system under the impact load.

From Fig.12, the following equivalent damping parameters can be obtained and summarized in Table 3.

Table 3. Equivalent damping parameters of the main drive system.

	Value		Logarithmic decrement rate δ	Damping ratio of main drive system ξ
	t_i	t_{i+T}		
velocity v_6	1.601	1.038	0.433	0.069
acceleration a_6	4.689	2.773	0.436	0.069

According to the parameters obtained in Table 3, the value of the damping ratio of the main drive system is about 0.069. Therefore, it can be taken as 0.069. It is also known that the total mass of the main drive system is 2592kg. According to the Eq.(23)-(25), the equivalent damping value of the main drive system can be obtained as c_6=1.28e5。

After obtaining the parameters of each part, the vibration mechanical model of the controlled object can be finally established, and used in the active vibration control simulation.

3 Numerical simulation and discussion

3.1 Analog excitation input

Because the effect of the vertical excitation force on the forming accuracy is the most direct and the largest, the reference excitation force input of the active vibration control can be composed of the blanking force excitation during the FB process and the unbalanced inertia force excitation during the non-working process. In order to simulate the error during the actual active vibration control process, the random

vibration interference is added to the reference excitation input. The reference excitation force input is shown in Fig.13.

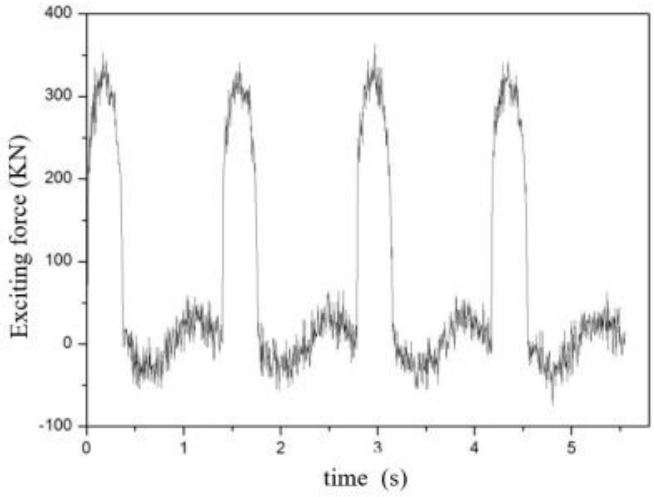

Fig.13. Reference excitation force input.

4.2 Reference input based on the measured vibration response

4.2.1 Vibration measurement scheme of fine blanking machine

The composition of the vibration measurement system of the mechanical servo FB press can be depicted by the schematic diagram shown in Fig.14. During the working process, the vibration at the working area is the most obvious, which have a direct impact on the forming accuracy. Therefore, the vibration at the working area needs to be measured. Meanwhile, the rigidity of the frame in the middle area is much smaller than that of the upper and lower crossbeams, and the guide rail of the slide block is arranged on the frame column in the middle area. Therefore, measuring points need to be arranged on the inner side of the stand column to reflect the vibration mode of the whole machine. Therefore, the measuring points arranged at the worktable area of the FB press are shown in Fig.15, and 12 three-way acceleration sensors are even distributed at the working area.

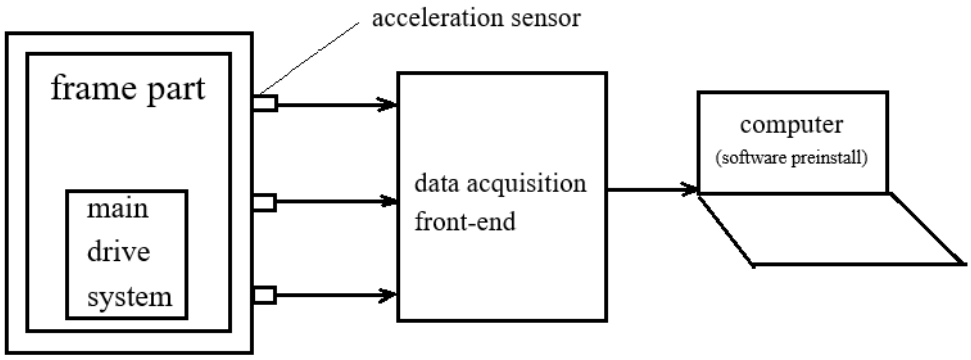

Fig.14. Vibration measurement schematic diagram.

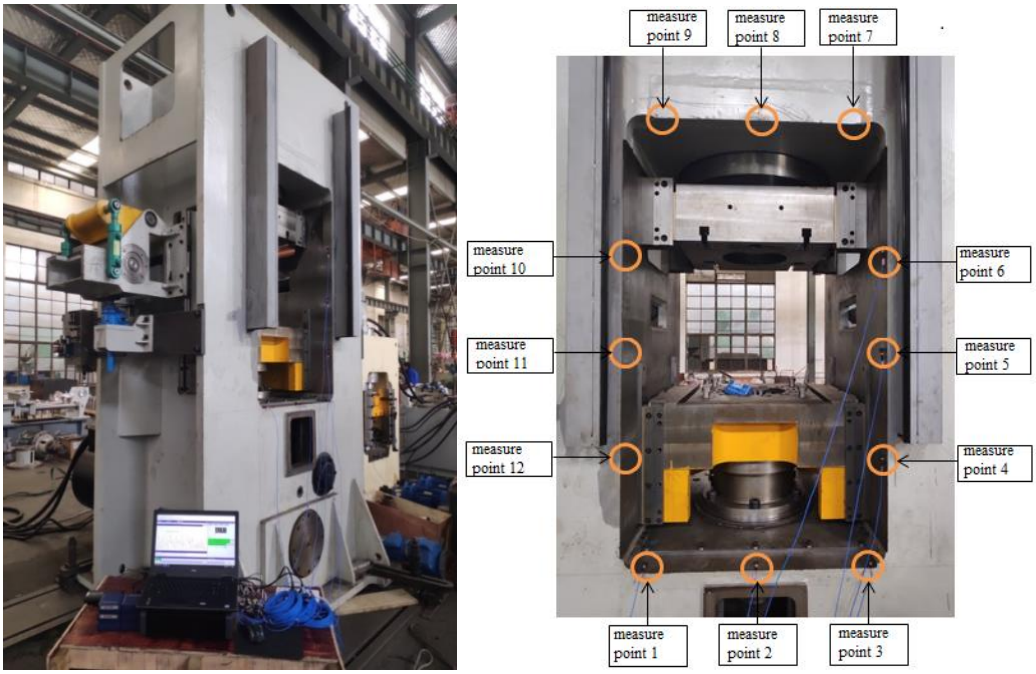

Fig.15. Measuring points distribution at the working area.

4.2.2 Test results of measuring points

During the test, the mechanical servo FB press works periodically with the speed of 87 times per minute under the no-load condition. In the movement process, the inertial load affects the lower crossbeam directly, and the vibration will be transmitted to the worktable, resulting in the forming error. The bottom of the lower cross-beam connected with the ground by installation system, the overall stiffness is very large. Therefore, the acceleration response of measuring points 1, 2 and 3 can reflect the overall response of the lower crossbeam, which shown in Fig.16.

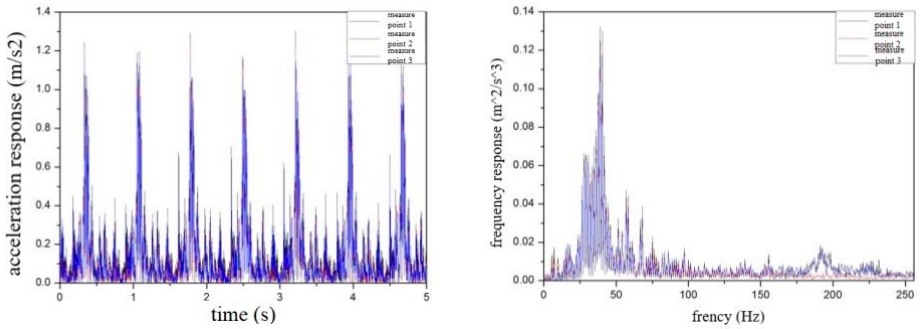

(a) Time domain response diagram (b) Frequency domain response diagram

Fig.16. Response of Z-direction time domain and frequency domain of measuring points at the lower cross beam area (measuring points of 1, 2 and 3).

Compared with the upper and lower crossbeams, the rigidity of the frame columns on the left and right sides in the middle is smaller, and the deformation will have a great impact on the whole press deformation. As the left and right columns are of symmetrical structure, the deformation situation is similar from the results, so the deformation situation on the right side is selected to do the analysis. The response situations in time domain and frequency domain are shown in Fig.17.

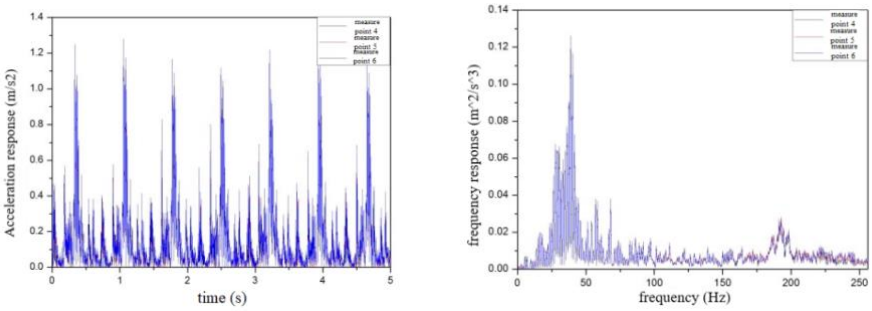

(a) Time domain response diagram (b) Frequency domain response diagram

Fig.17. Response of Z-direction time domain and frequency domain of measuring point at frame column area (measuring points of 4, 5 and 6).

The overall rigidity of the upper crossbeam is very large. Because the upper crossbeam is far away from the frame installation system, it is easy to produce large vibration response. The response situations in the time and frequency domain are shown in Fig.18.

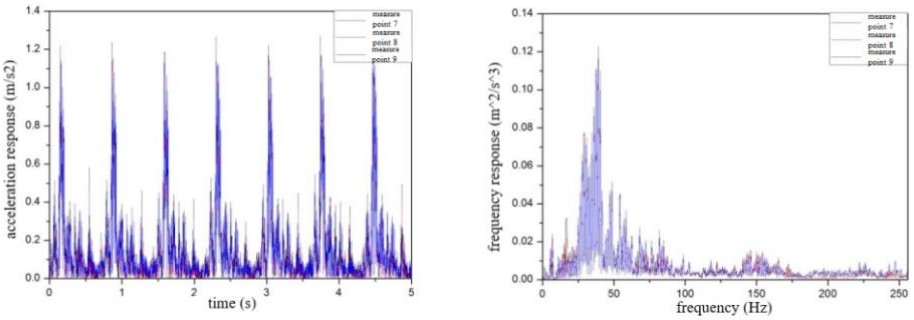

(a) Time domain response diagram (b) Frequency domain response diagram

Fig.18. Response of Z-direction time domain and frequency domain of measurement point at upper crossbeam area (measuring points of 7, 8 and 9).

3.3 Numerical simulation results

According to the self-adaptive vibration feed forward control method as described in Section 2, the control system simulation process is programmed in Matlab software platform, and the value of μ_k is 0.005, γ is 10e-5. Combined with the mechanical model of the controlled object, the time-domain vibration response of each observation point with and without control can be obtained, as shown in Fig.19a. The simulation results show that the control effect of all measuring points is very good, so we use measuring point 2 to show. The frequency domain vibration response of observation point 2 with and without control can be obtained, as shown in Fig.19b.

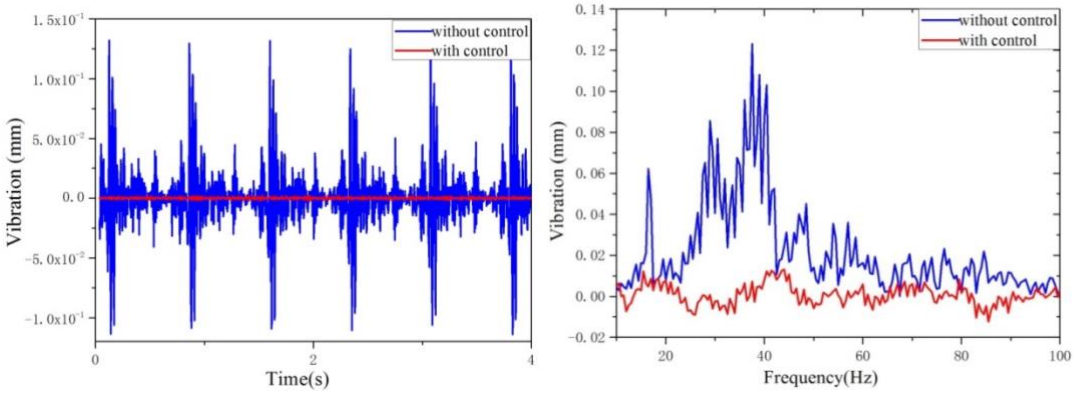

Fig.19. a) time domain and b) frequency domain vibration response with and without control.

In Fig.19, the blue line represents the vibration response output without control, and the red line represents the vibration response output adding active control. It can be seen from the Fig.19 that the vibration response of the press with the active vibration control is effectively reduced. The time-domain vibration response quickly achieves stability when the active control applied, and the convergence speed is very fast, which means that it has a stable control effect at this time. It can be seen that the

vibration of the frame has been significantly suppressed, and the maximum value of the vibration response has been reduced by more than 95%, the amplitude variation of the vibration response is maintained within the range of 1e-5m.

For the frequency domain control effect, it can be seen that after controlling the corresponding response of the first three modes, the vibration response amplitude reaches to stable very fast, and the maximum value of the vibration response is reduced by more than 80%. At the same time, the convergence speed of the system is very fast after the application of active vibration control.

From the simulation results, it can be seen that the active vibration control applied to the FB press does not suppressed the vibration completely. However, the effect of vibration control is very significant, which shows a promising future for the application of the active vibration control method on the FB press.

4 Conclusion

The self-adaptive feed forward control is used to simulate the vibration control of the mechanical FB press. The simulation results show that the vibration control effect is good, and the conclusion can be obtained in the following:

(1) The principle of vibration control of fine blanking press is described, the control algorithm is established, and the adaptive vibration control block diagram of fine blanking press is established.

(2) The vibration mechanical model of the fine blanking press as the controlled object is established, and the parameters of the excitation input and the mechanical model are calculated.

(3) The vibration response of the whole machine has been effectively reduced when the active control is applied, in which the time-domain vibration response has been reduced by more than 95%, and the frequency-domain vibration response has been reduced by more than 80%, which means that the vibration reduction effect is obvious.

5 Declaration

5.1 Availability of data and materials

The datasets used and/or analysed during the current study are available from the corresponding author on reasonable request.

5.2 Competing interests

The authors declare that they have no competing interests

5.3 Funding

Fundamental Research Funds for the Central Universities (WUT: 2019ⅢⅢ117CG) , 111 Project（B17034）and Innovative Research Team Development Program of Ministry of Education of China (No. IRT_17R83) give to this research supports and the Huangshi Huali Metal forming Machine Tool Co., Ltd. give to experiments supports.

5.4 Authors' contributions

YL guide the experiment, YS was a major contributor in writing the manuscript, WH did the main experiment, ZX and XZ helped experiment. All authors read and approved the final manuscript.

5.5 Acknowledgements

The authors would like to thank the Fundamental Research Funds for the Central Universities (WUT: 2019ⅢⅢ117CG) , 111 Project（B17034）and Innovative Research Team Development Program of Ministry of Education of China (No. IRT_17R83) for the supports given to this research and the Huangshi Huali Metal forming Machine Tool Co., Ltd. for their supports given to experiments.

References

[1] Liu Y, Tang B, Hua L, et al, (2018). Investigation of a novel modified die design for fine-blanking process to reduce the die-roll size, Journal of Materials Processing Technology, 260,30-37.

[2] Mao H, Li S, Liu Y, et al, (2017). An investigation on the microstructure of the fine-blanked sprocket, The International Journal of Advanced Manufacturing Technology, 90,3171-3185.

[3] Xu Z, Liu Y, et al, (2019). Energy analysis and optimization of main hydraulic system in 10,000 kN fine blanking press with simulation and experimental methods, Energy Conversion and Management, 181,143-158.

[4] Zhao X, Liu Y, Hua L, et al, (2016). Finite element analysis and topology optimization of a 12000KN fine blanking press frame, Structural and Multidisciplinary Optimization, 54,375-389.

[5] Nagamatsu Akio, SOKCHU, P. (1993). Vibration analysis and structural optimization of a press machine, Finite Elements in Analysis and Design - FINITE ELEM ANAL DESIGN, 14,297-310.

[6] Winberg Mathias, Johansson Sven, Lag Thomas. ACTIVE CONTROL OF ENGINE INDUCED NOISE IN A NAVAL APPLICATION[C]. Hong Kong, China.

[7] Changjian S, Zhang X, Yun W. (2000). Active vibration controller designing for high-speed flexible linkage mechanisms, Chinese Journal of Mechanical Engineering, 36,54-58.

[8] Li, P. (2012). Theoretical Anlysis and Experiment on Active Vibration Control of a Shaft-hull System, Journal of Mechanical Engineering, 48,103.

[9] Zhu M, Jin G, Feng N. (2011). Numerical Study of Active Control of Interior Noise in a Structural-Acoustic Enclosure, Key Engineering Materials, 486,103-106.

[10] Teo Yik R, Fleming, Andrew J. (2015). Optimal integral force feedback for active vibration control, Journal of Sound and Vibration, 356,20-33.

[11] Park Young-min, Kim Kwang-joon, (2013). Semi-active vibration control of space truss structures by friction damper for maximization of modal damping ratio, Journal of Sound Vibration, 332,4817-4828.

[12] Sun W, Zhang F, Luo S, et al. (2017). Simulation analysis of adaptive active vibration control[J]. Sound and vibration control.37,23-28.

[13] Beredugo Y, Novak M, (2011). Coupled Horizontal and Rocking Vibration of Embedded Footings, Canadian Geotechnical Journal, 9,477-497.

[14] Novak M. (1974). Effect of soil on structural response to wind and earthquake, Earthquake Engineering & Structural Dynamics, 3,79-96.

[15] Novak M. (2011). Foundations for shock-producing machines, Canadian Geotechnical Journal, 20,141-158.

Biographical notes

Yan-Xiong Liu, born in1985, Associate Professor, School of automotive engineering, *Wuhan University of Technology*, *Hubei Key Laboratory of Advanced Technology of Automotive Components.*; E-mail: liuyx@whut.edu.cn.

Yu-Wen Shu, born in 1997, Graduate student, School of automotive engineering, *Wuhan University of Technology, Hubei Key Laboratory of Advanced Technology of Automotive Components.*;E-mail:1543380083@qq.com

Wen-Tao Hu, born in 1995, Graduate student, School of automotive engineering, *Wuhan University of Technology, Hubei Key Laboratory of Advanced Technology of Automotive Components.*; E-mail: wentaohu.whut@qq.com

Xin-Hao Zhao, born in 1989, Ph.D. School of automotive engineering, *Wuhan University of Technology, Hubei Key Laboratory of Advanced Technology of Automotive Components.*; E-mail: zhaoxh@whut.edu.cn

Zhi-Cheng Xu, born in 1994, Ph.D. School of automotive engineering, *Wuhan University of Technology, Hubei Key Laboratory of Advanced Technology of Automotive Components.*; E-mail: Xuzhicheng@whut.edu.cn

Figures

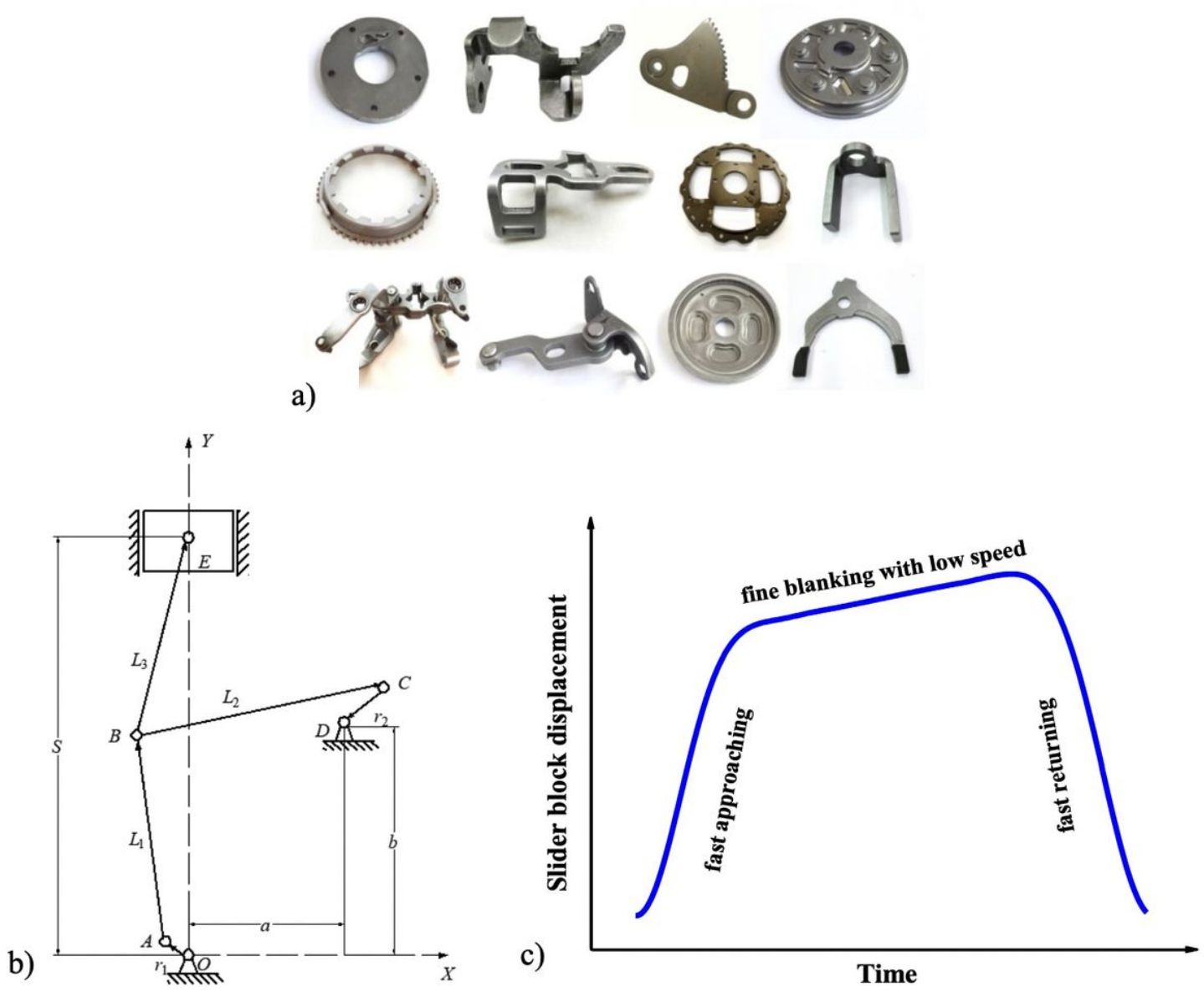

Figure 1

a) the mid-thick sheet metal parts fabricated by FB process, b) the mechanical construction of the main driving system of the high speed FBFB press and c) the slide block stroke diagram.

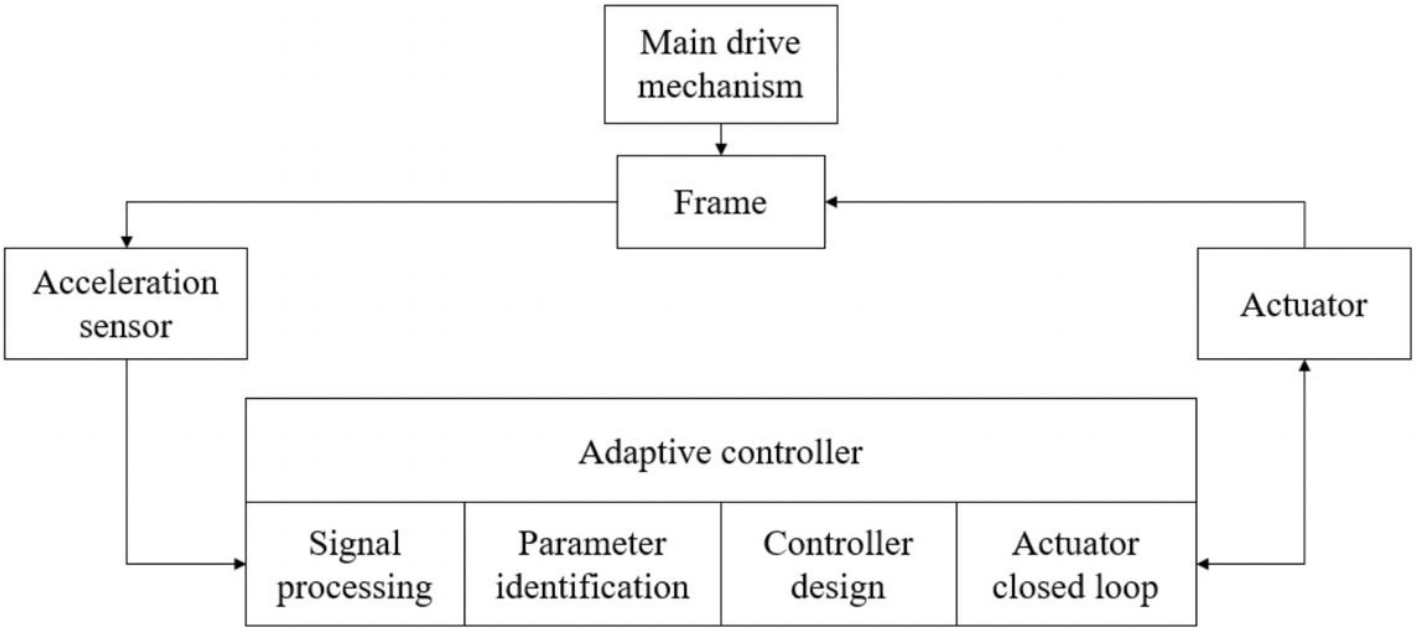

Figure 2

Schematic diagram of the active vibration control system for FB press.

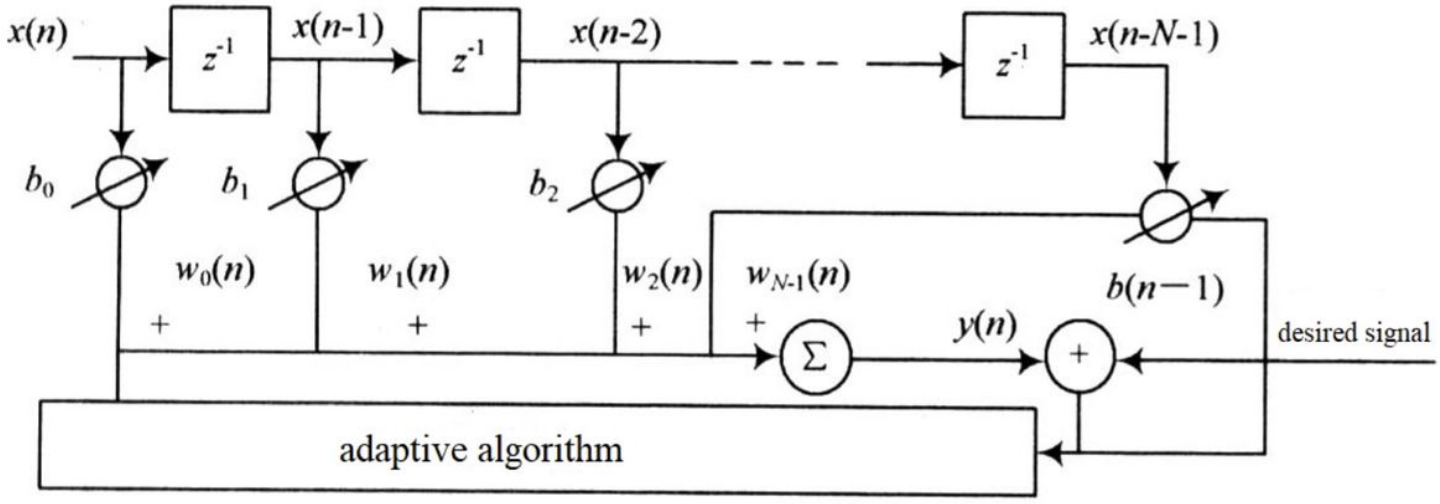

Figure 3

Adaptive FIR filter.

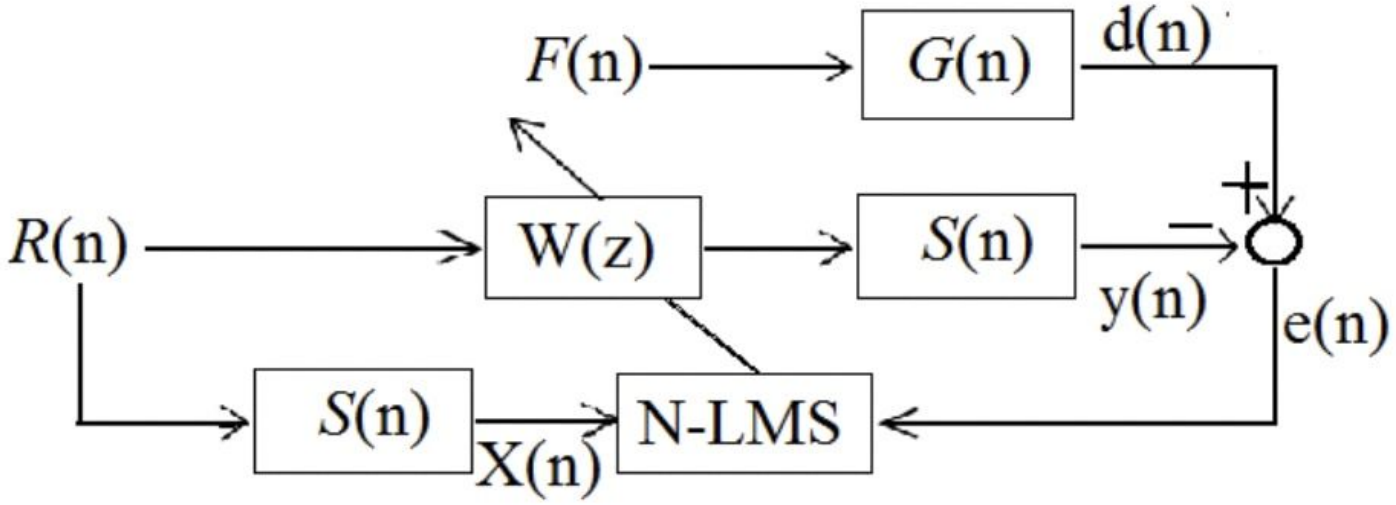

Figure 4

Active vibration control block diagram of the FB press.

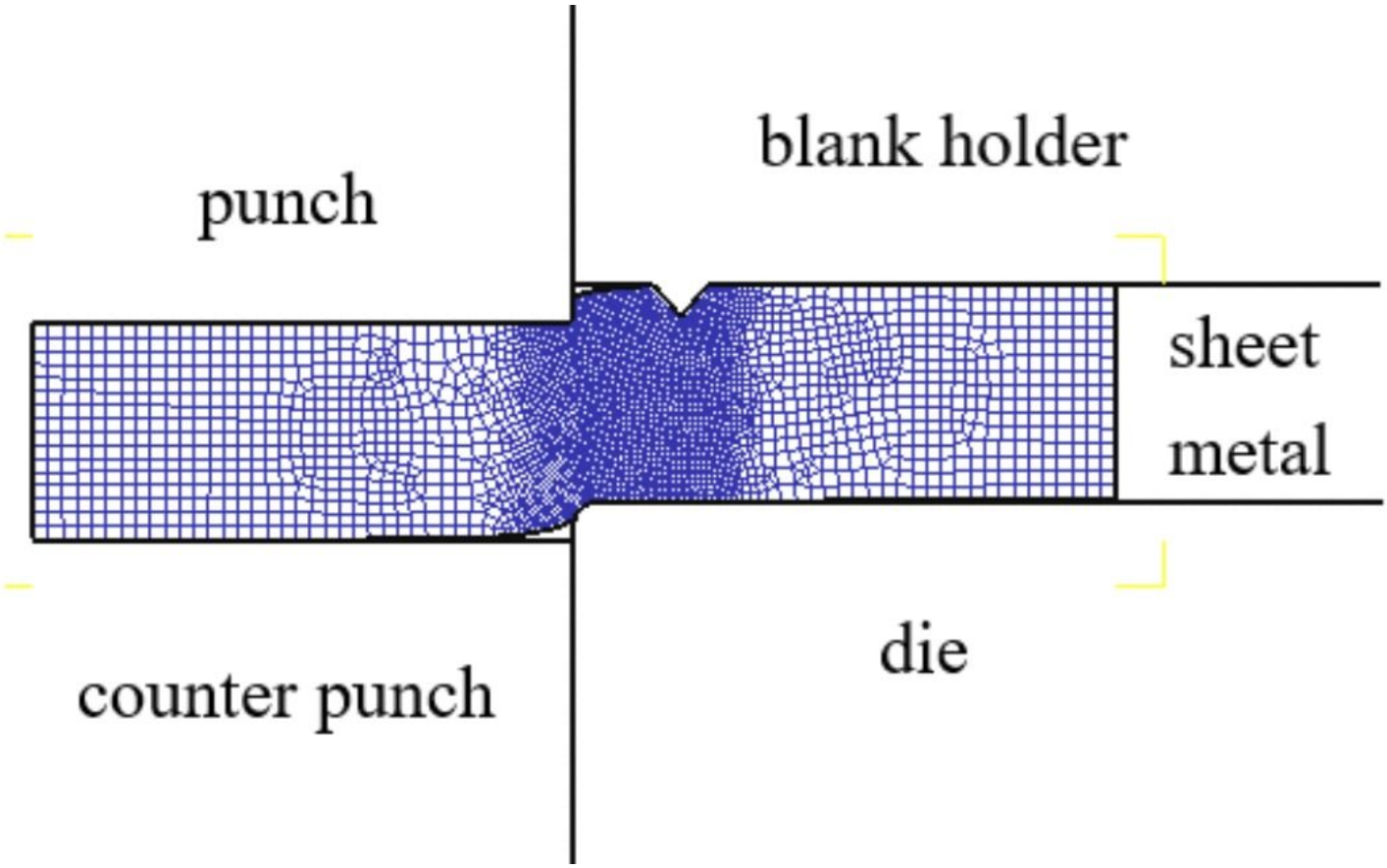

Figure 5

The FE model of the FB process.

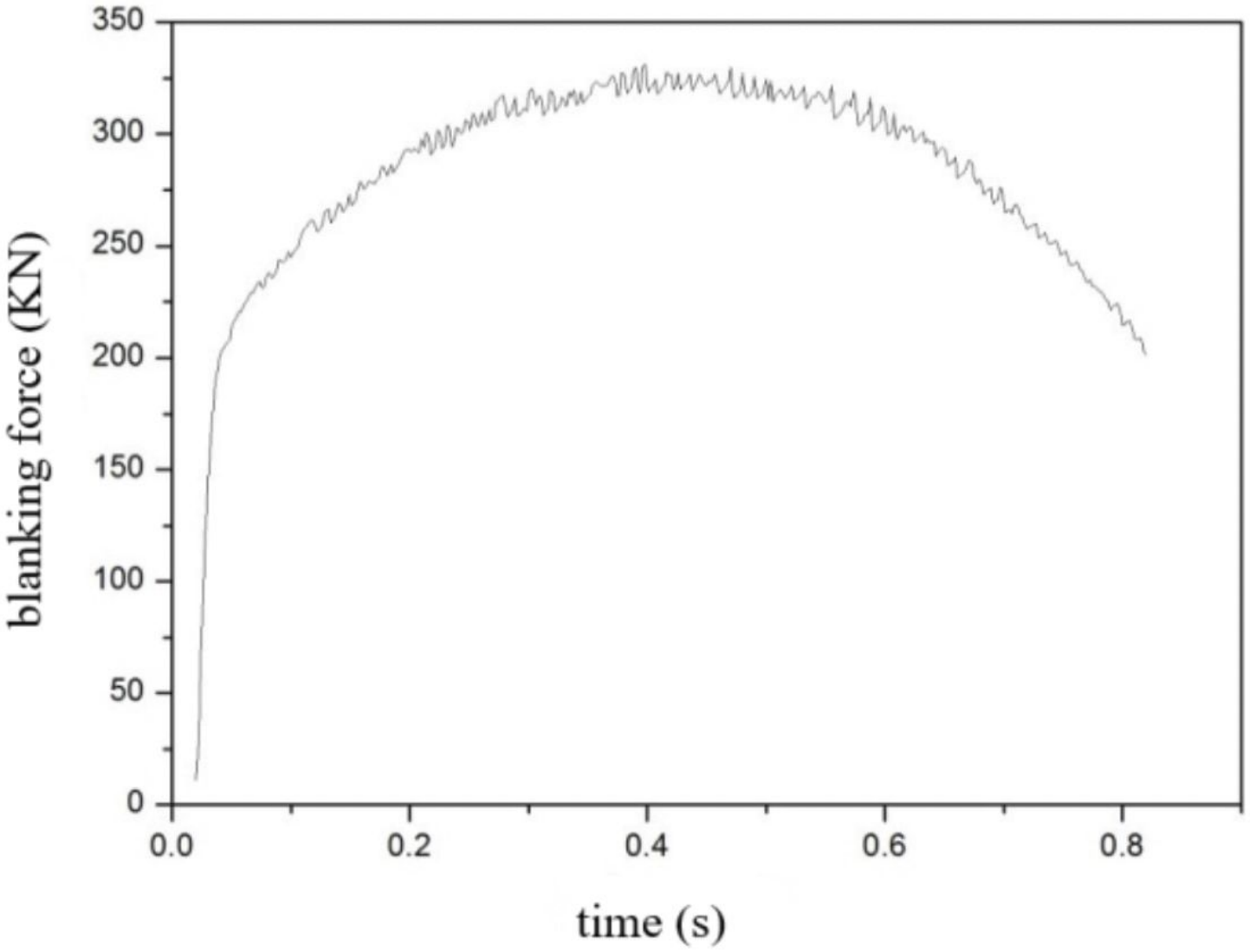

Figure 6

The relationship between the fine-blanking force and the time.

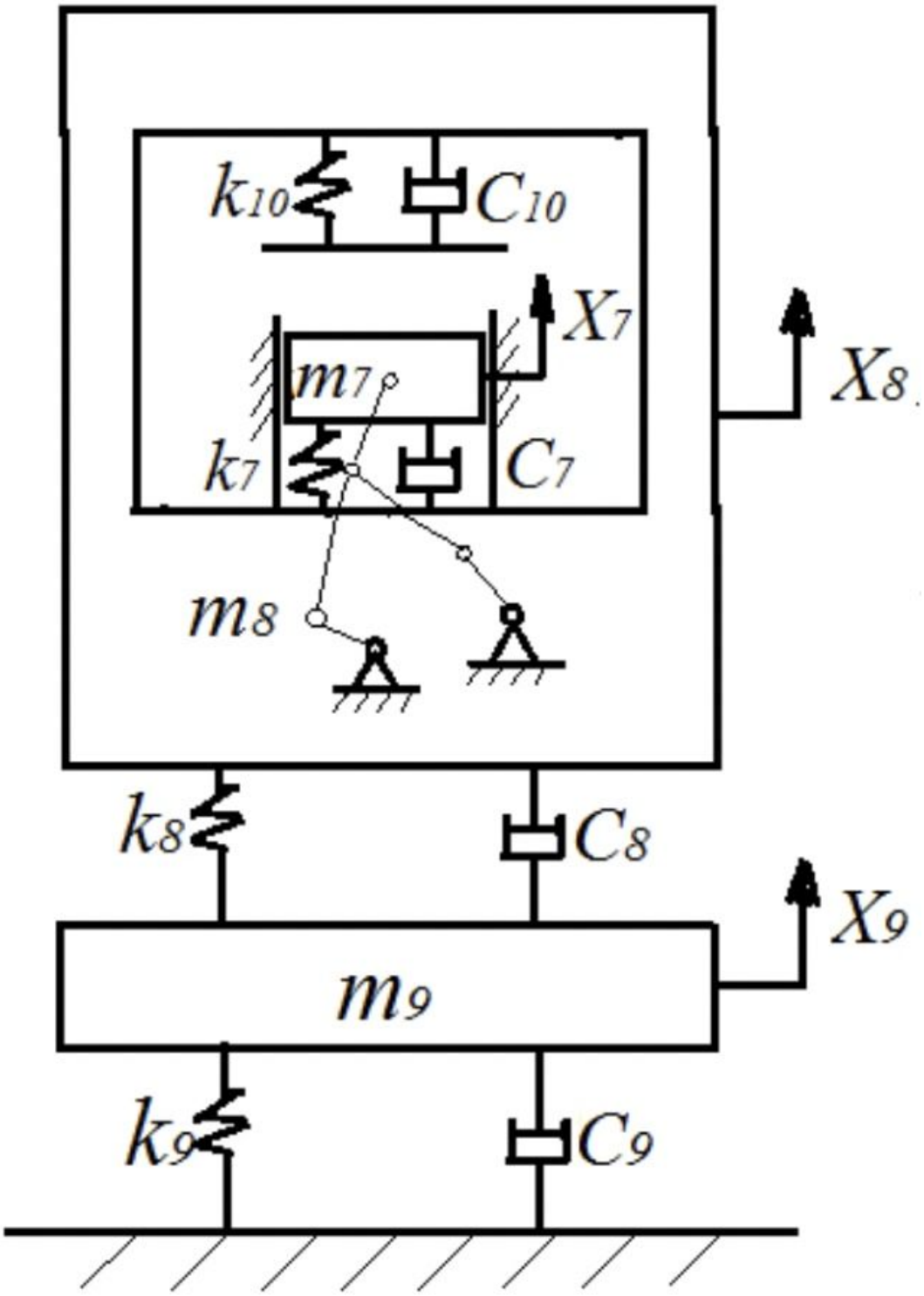

Figure 7

Vibration mechanical model of the FB press.

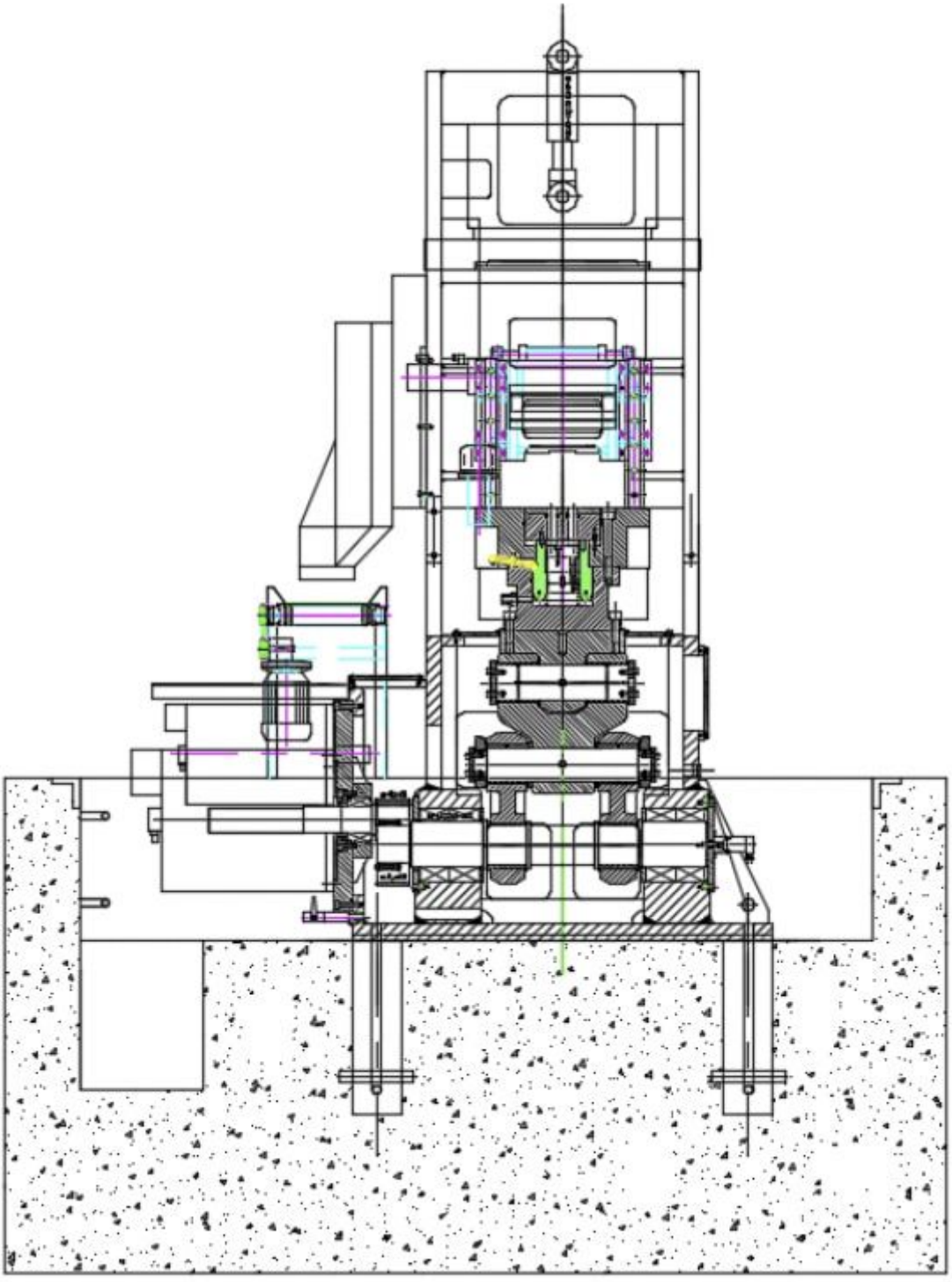

Figure 8

Foundation installation design of mechanical fine blanking machine

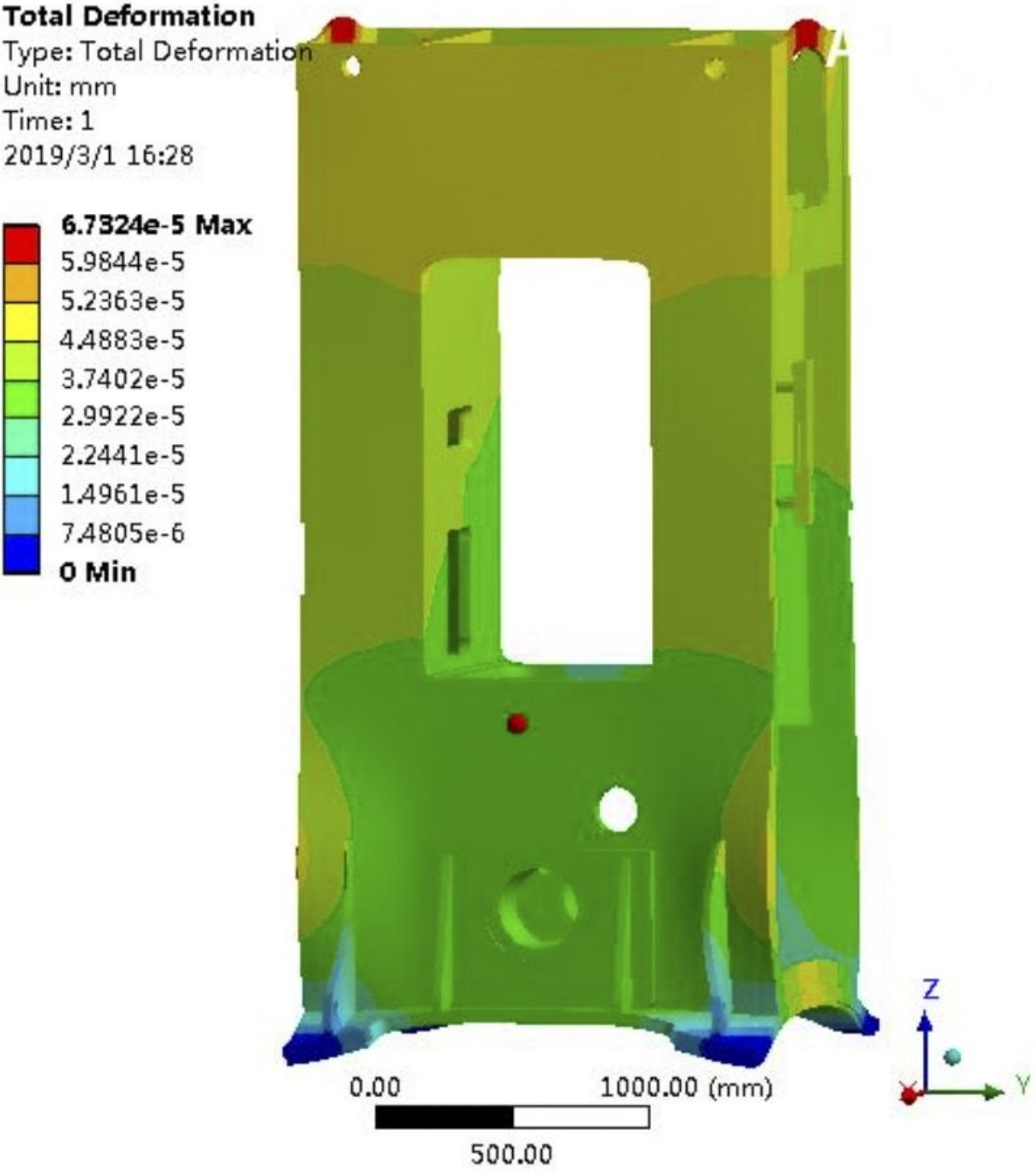

Figure 9

Frame deformation under the action of the constant load.

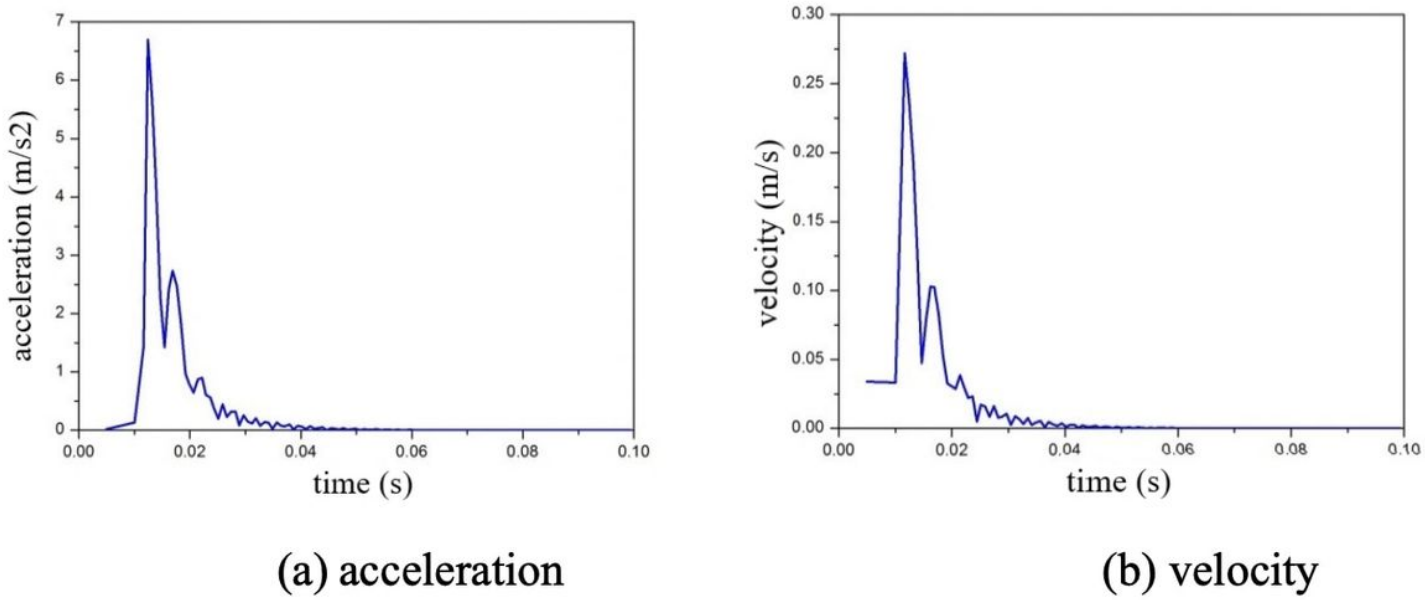

Figure 10

Acceleration and velocity attenuation on the frame under the impact load.

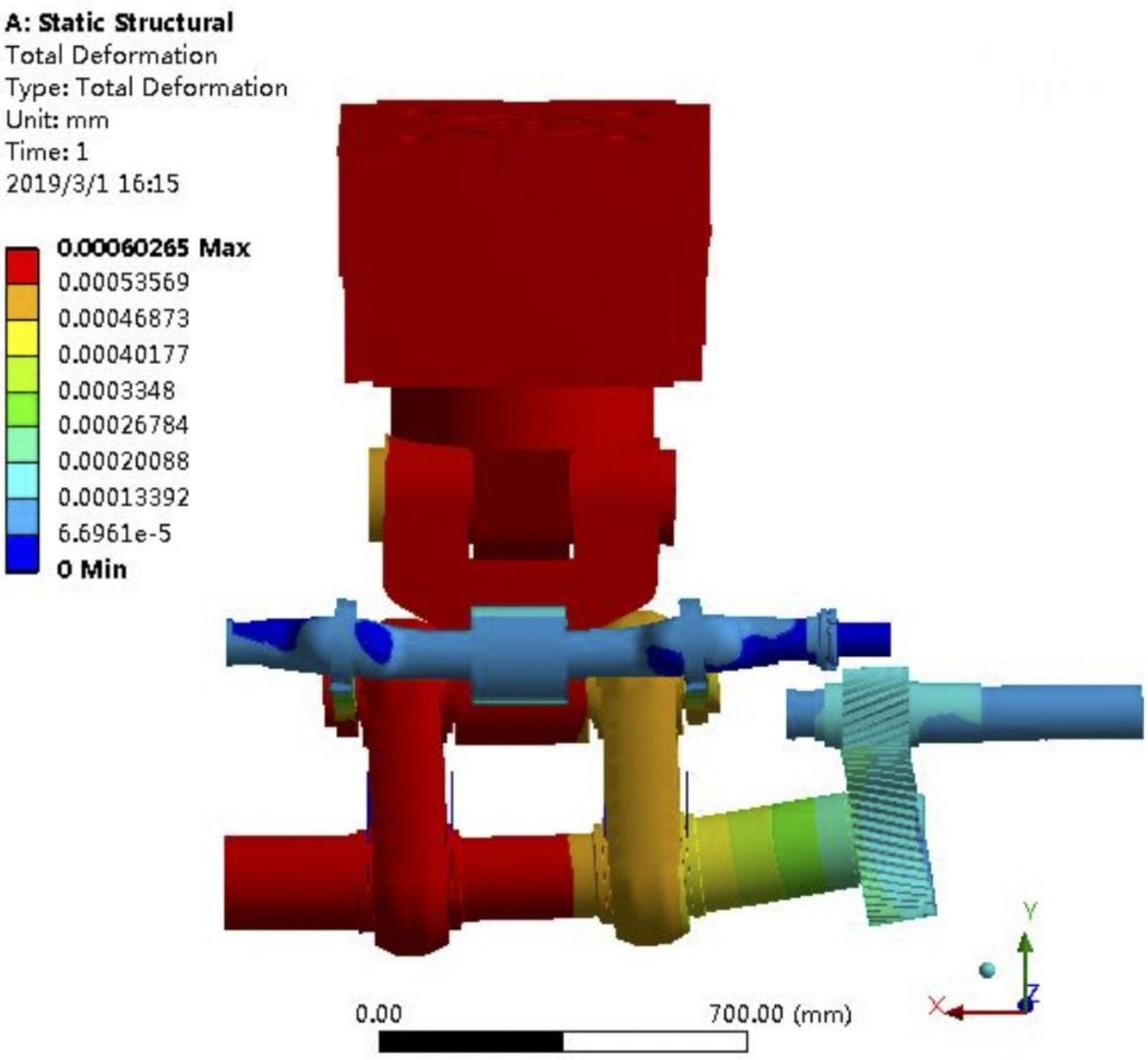

Figure 11

Deformation of the main drive system under the constant load.

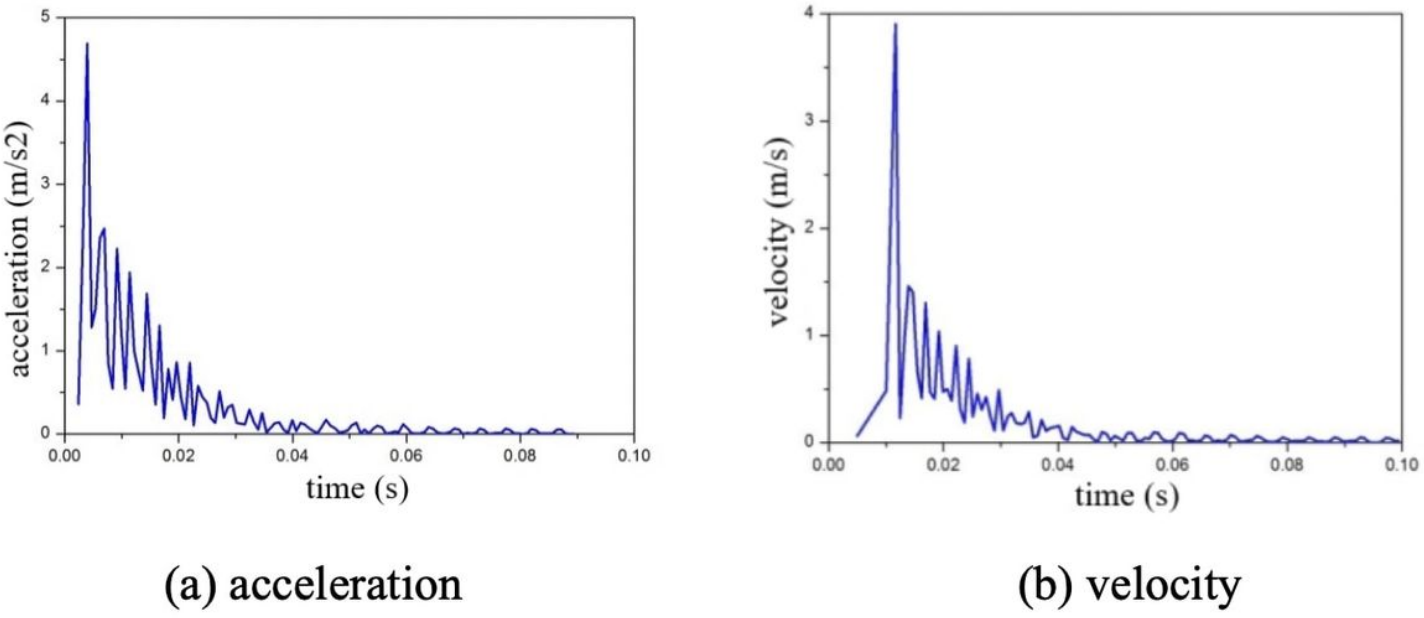

Figure 12

Acceleration and velocity attenuation of the main drive system under the impact load.

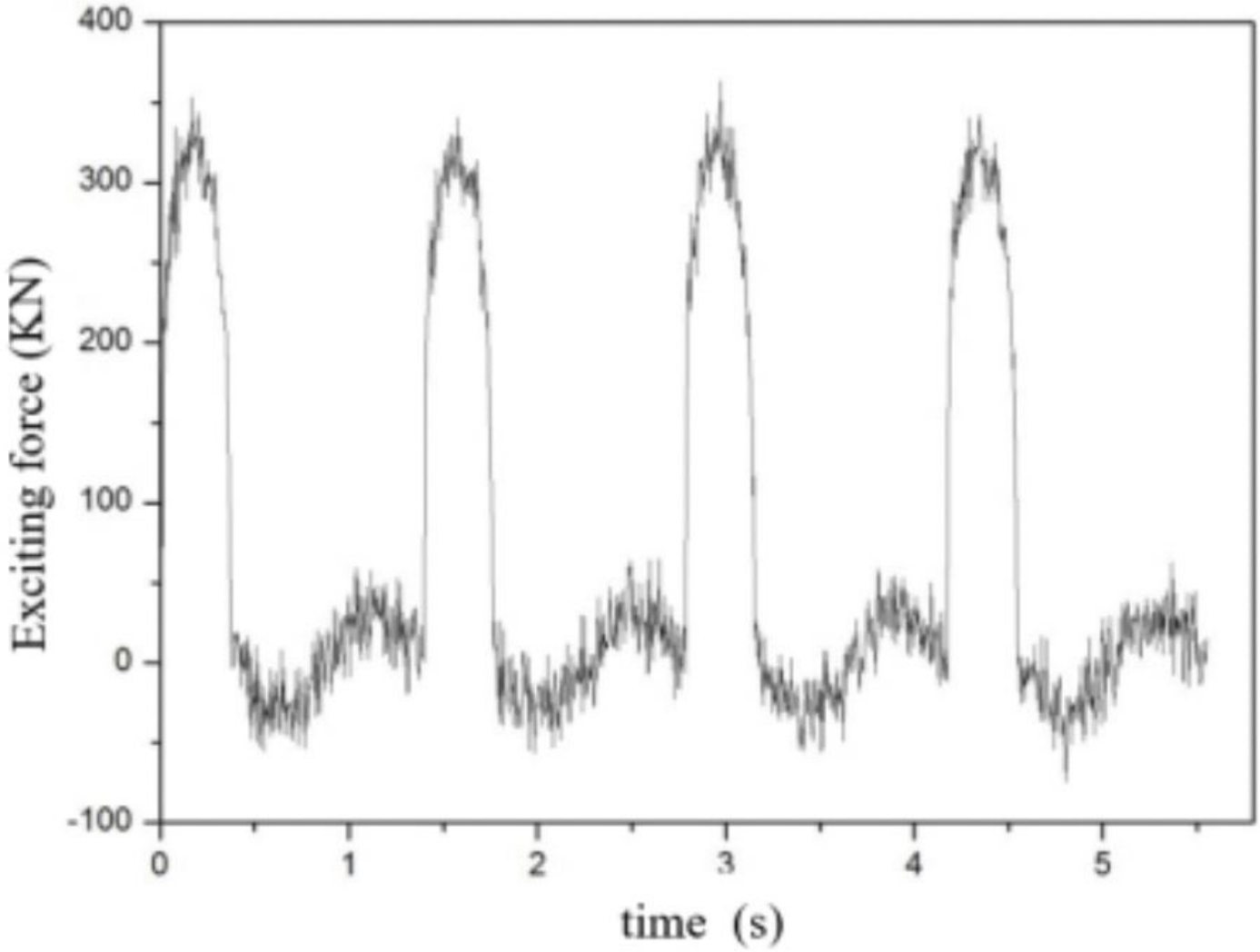

Figure 13

Reference excitation force input.

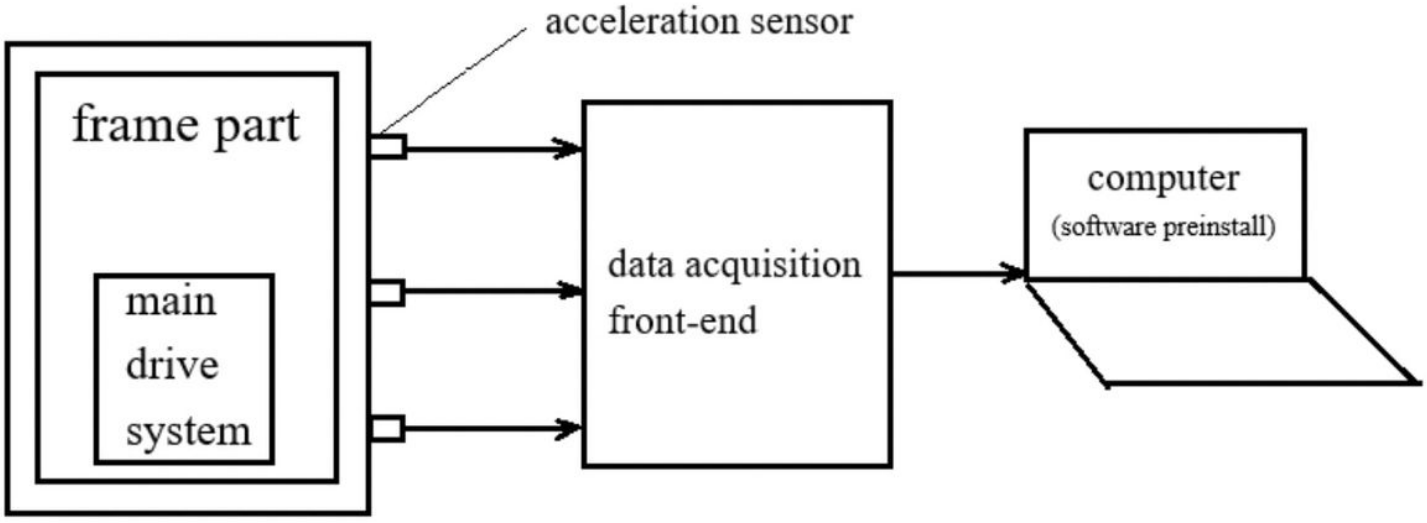

Figure 14

Vibration measurement schematic diagram.

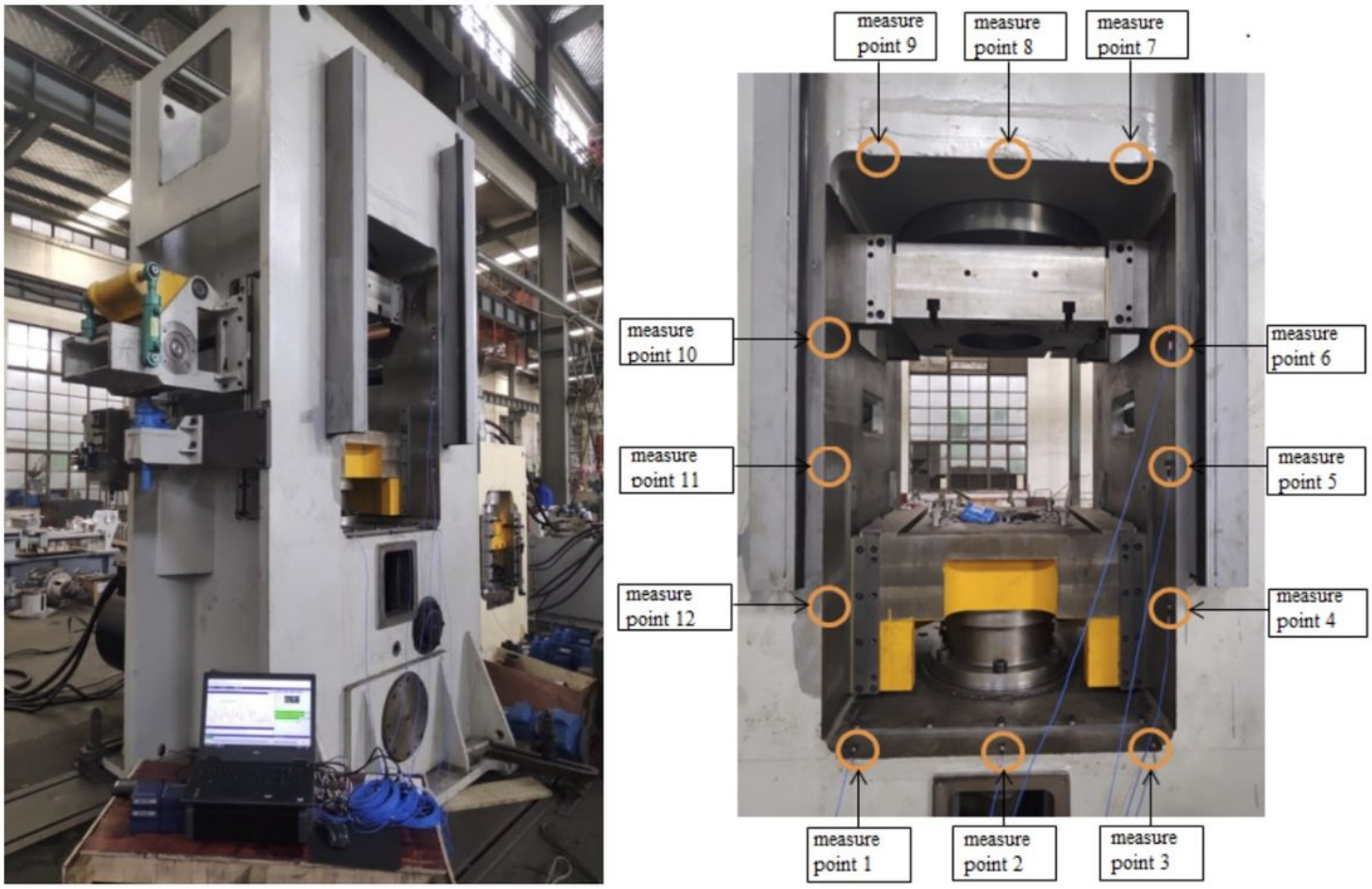

Figure 15

Measuring points distribution at the working area.

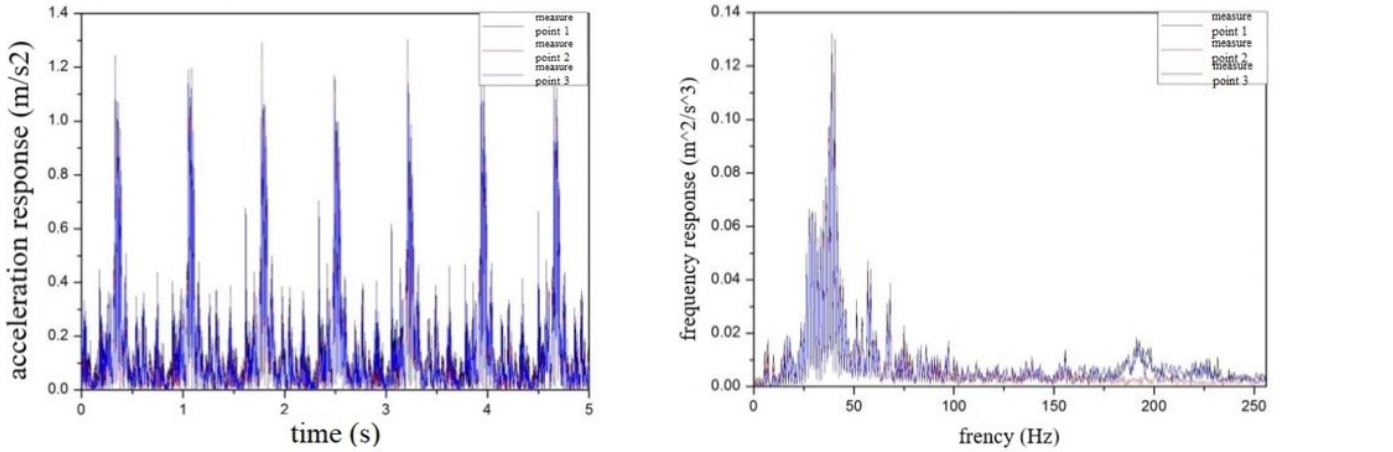

(a) Time domain response diagram

(b) Frequency domain response diagram

Figure 16

Response of Z-direction time domain and frequency domain of measuring points at the lower cross beam area (measuring points of 1, 2 and 3).

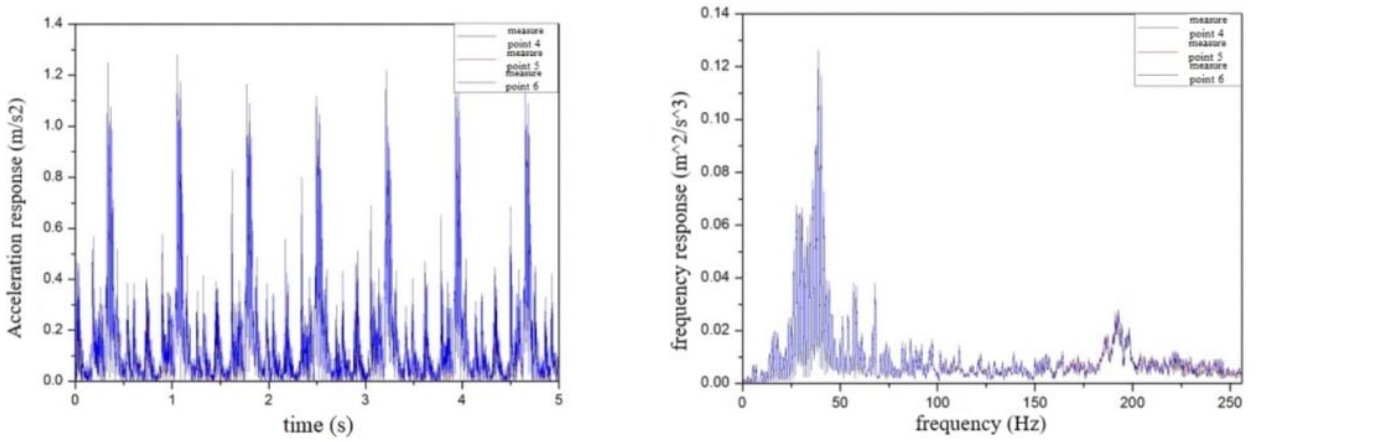

(a) Time domain response diagram (b) Frequency domain response diagram

Figure 17

Response of Z-direction time domain and frequency domain of measuring point at frame column area (measuring points of 4, 5 and 6).

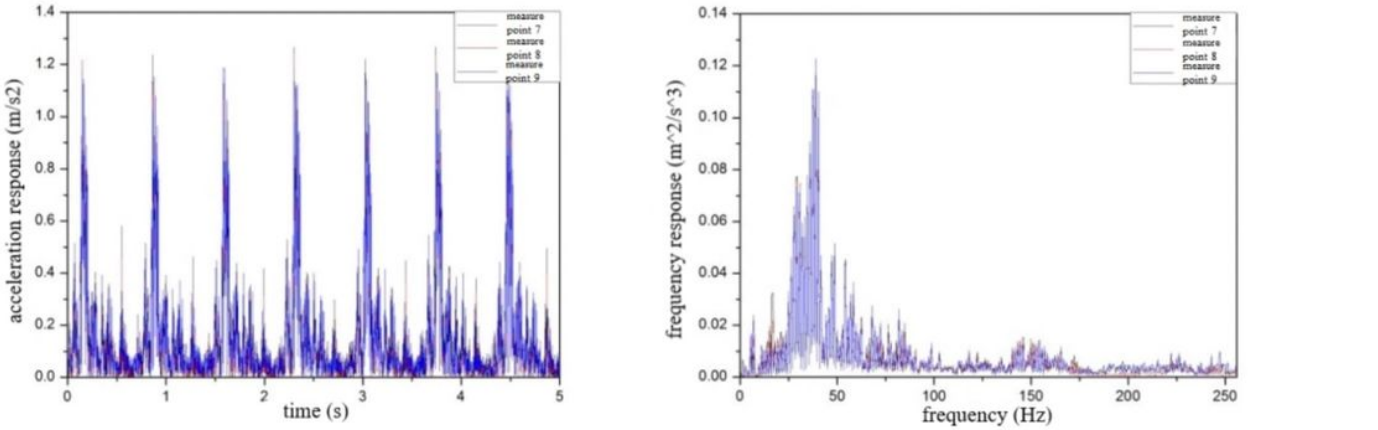

(a) Time domain response diagram (b) Frequency domain response diagram

Figure 18

Response of Z-direction time domain and frequency domain of measurement point at upper crossbeam area (measuring points of 7, 8 and 9).

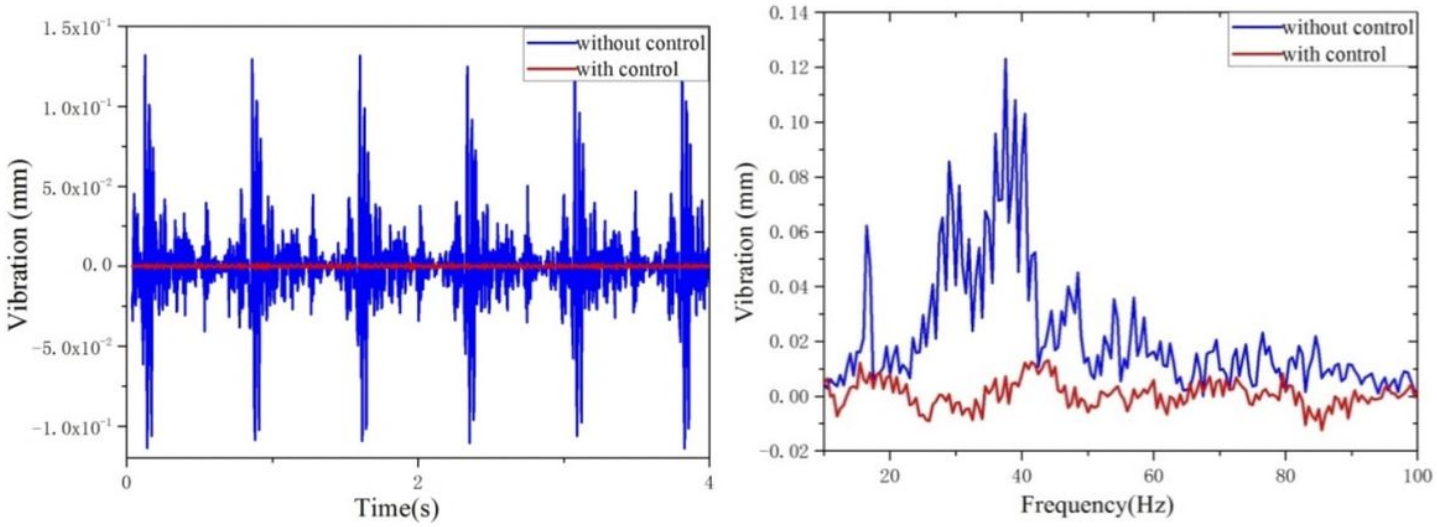

Fig.19. a) time domain and b) frequency domain vibration response with and without control.

Figure 19

a) time domain and b) frequency domain vibration response with and without control.